

Article

Minerals and Enrichment of W, Rb, and Cs in Late Permian Coal from Meitian Mine, Meitian Coalfield, Southern China by Magmatic Hydrothermal Fluids

Zhenghui Xiao ^{1,2,*}, Yunjiang Cao ¹, Wei Jiang ^{1,2}, Ping Zhou ³, Yanran Huang ^{1,2}  and Jisong Liu ¹

¹ School of Resource, Environment and Safety Engineering, Hunan University of Science and Technology, Xiangtan 411201, Hunan, China; caoyj-xt@sohu.com (Y.C.); jiangwei3q@163.com (W.J.); hyanran2006@hnust.edu.cn (Y.H.); ljs930106@163.com (J.L.)

² Hunan Key Laboratory of Shale Gas Resource Exploitation, Hunan University of Science and Technology, Xiangtan 411201, Hunan, China

³ School of Economics, Hunan Institute of Engineering, Xiangtan 411104, Hunan, China; zhouping2010@163.com

* Correspondence: xiaozhenghui2003@163.com; Tel.: +86-731-5829-0040

Received: 22 September 2018; Accepted: 31 October 2018; Published: 5 November 2018



Abstract: We report on the effects of magmatic hydrothermal fluids on the mineralogical and geochemical compositions of 12U and 12L Coals from the Meitian Mine in the Meitian Coalfield, southern China. The minerals in 12U Coal are predominantly chlorite, quartz, and calcite, while the minerals in 12L Coal consist mainly of illite, quartz, chlorite, kaolinite, and mixed-layer illite/smectite (I/S). The vesicle- and fracture-filling illite, chlorite, I/S, pyrite, and fluorite, cleat- and fracture-filling carbonate minerals (i.e., calcite, and dolomite), and cleat-filling tremolite, diopside, and talc have epigenetic hydrothermal origins. Tremolite, diopside, and talc were probably formed from the reaction between dolomite and Si-rich magmatic hydrothermal fluids. Elevated Pb–Zn–Sn–Cd assemblages are characteristic for the 12U Coal, while 12L Coal is enriched in W, Rb, Cs, Th, V, Zn, and Zr, most notably W, Rb, and Cs. REY (Rare Earth Elements and Yttrium) plots for almost all coals, partings and host rocks are similar, showing an M-type REY distribution, Gd-maximum, positive Y anomalies, and negative Ce anomalies, suggesting acid hydrothermal circulation in the coal-bearing strata. Rubidium and cesium in the coal is clearly associated with K-rich clay minerals (illite + I/S), and to a lesser extent with silicate minerals that were precipitated from hydrothermal solutions. W in the coals mainly occurs in the inorganic constituents of illite and pyrite, especially illite. Enrichment of W, Rb, and Cs in the coal and host rocks is genetically associated with magmatic hydrothermal fluids. Specifically, magmatic hydrothermal fluids of relatively high temperatures that are rich in volatile matter can extract abundant W, Rb, and Cs from granitic melts. The enrichment of these rare metals in the coal is mainly related to illitization. Our study results suggest that, for coal intruded by magmatic rocks, the type of hydrothermal alteration may greatly influence the enrichment of elements.

Keywords: South China; rare metals; Meitian Coalfield; magmatic hydrothermal fluid; illitization; coal

1. Introduction

Some rare metals can be significantly enriched in coals and coal-bearing strata under specific geological conditions [1–3]. In recent years, metalliferous coal deposits that contain very high concentrations of rare metals have attracted substantial attention due to the recovery potential of critical elements from them [1,2,4–8].

Magmatic intrusions are common in coal seams [9,10]. Some study results showed that magmatic intrusions can lead to some physical and chemical changes of coal, such as the formation of mosaic and vesicular structures, an increase or decrease in gas content and adsorption capacity, and the formation of anisotropic components (e.g., epigenetic minerals), which have positive or negative effects on coalbed methane development [11–14].

Many study results showed that magmatic intrusions greatly influence petrographic, geochemical and mineralogical compositions of coal seams [9,10,15–22]. Previous studies have shown that some zoned distributions of coal ranks are highly associated with igneous intrusions worldwide, and many elements enriched in coals are derived from magmatic and hydrothermal inputs [9,10,17–24]. More specifically, Querol et al. (1997) [9] showed that coals from the Fuxin Basin, China, are rich in manganese because of a diabase intrusion. Finkelman et al. (1998) [10] showed that some rare metals, such as Rb, Mo, U, Ga, and Ge, are concentrated in coal from Pitkin County, Colorado, and the primary carriers of these rare metals in coals are clay minerals and/or organic matter. Golab et al. (2004) [17] showed that, at the contact between coal and intrusion, some elements (e.g., V, Sc, Sm, Rb, Pb, S) are enriched in thermally altered coals from Upper Hunter Valley, Australia. Suárez-Ruiz et al. (2006) [18] reported that Mn and V in the coals from Rio Maior (Portugal) and Peñarroya (Spain) Basins are related with the circulation of magmatic fluids. Dai and Ren (2007) [19] attributed elevated concentrations of some elements (e.g., Zn, Pb, and U) in coal from Fengfeng-Handan coalfield, Hebei, China, to magmatic intrusions. Zheng et al. (2008) [20] and Dai et al. (2012) [21] showed that the increased Hg in the altered coals from Huaibei Coalfield, Anhui, and from Adaohai Mine, Inner Mongolia, was probably derived from igneous fluids. Chen et al. (2014) [22] showed that some elements (i.e., Fe, Ca, S, Si, Mg, Zn, Cd, and Pb) in coals from Pansan Mine of Huainan Coalfield, Anhui, China, were mainly sourced from magmatic hydrothermal fluids.

Some results indicated that certain epigenetic minerals in thermally altered coals, such as carbonate minerals (e.g., calcite and dolomite) and sulphide minerals (e.g., pyrite and pyrrhotite), mainly originate from hydrothermal alteration, and these minerals tend to carry some trace elements transported into altered coals by hydrothermal fluids [9,10,17–22,25]. Although the effects of igneous intrusions on petrographic, geochemical and mineralogical compositions of coal seams have been extensively studied, the mechanism of elements sourced from magmatic intrusions and then enriched in coal is not completely clear.

It is well known that Southern Hunan in South China hosts world-famous granitoid-related Cu–Pb–Zn and W–Sn polymetallic ore deposits [26]. The Meitian Coalfield is also located in this area, and the concentrations of some elements (e.g., W, Th, Nd, Rb, and U) in the coals may be associated with granitic intrusions [1,24]. However, minerals resulted from the granitic intrusions, the modes of occurrence of some elements enriched in the Meitian Coalfield and the major factors controlling their enrichment have not been investigated in detail.

In this study, we focus on the effect of magmatic hydrothermal fluids on the geochemical and mineralogical compositions of 12U and 12L Coals (late Permian) from the Meitian Mine in the Meitian Coalfield, southern Hunan, with particular focus on the modes of occurrence of rare metals, especially W, Rb, and Cs, and the major factors controlling their enrichment in the coals.

2. Geological Setting

Meitian Coalfield is located in the central Nanling region of the Cathaysian Block, South China (Figure 1a,b). An igneous intrusion, the Qitianling granite complex, is widely distributed in the north of the Meitian Coalfield (Figure 1b). This granite complex outcrops over an area of about 520 km² and ranges in age from Carboniferous to Early Triassic [27,28]. The zoned distribution of the coal rank in the Meitian Coalfield is completely related to magmatic hydrothermal intrusion, which resulted in Permian coals metamorphosing into bituminous, semianthracite, anthracite, meta-anthracite, and even graphite (Figure 1c) [24]. The studied coal beds are located in the metamorphic zone III (Figure 1c).

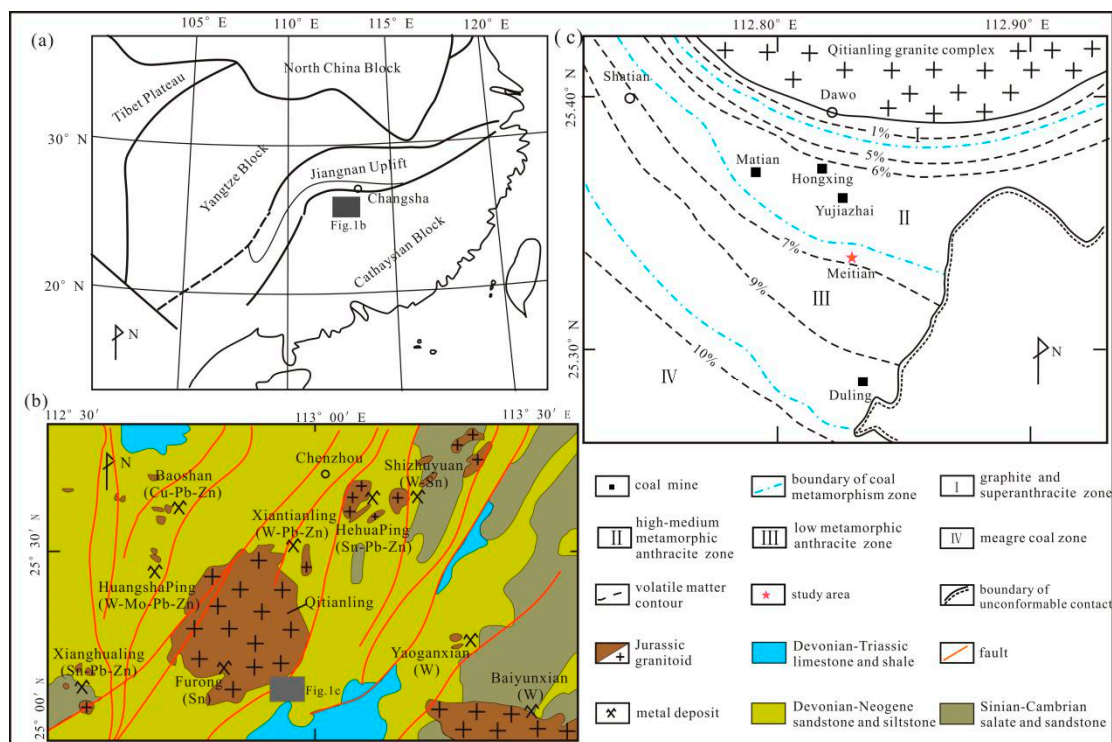


Figure 1. (a) Sketch map showing the regional geology of the central Nanling region, South China. (b) Distribution of Jurassic igneous rocks and associated polymetallic mineral deposits in the central Nanling region, South China, including the location of the Meitian Coalfield (modified from Li et al., 2007) [27]. (c) Schematic diagram showing metamorphic zones of the 12U and 12L Coals, including the location of the Meitian Mine (modified from Wang et al., 1999) [24].

The Meitian Mine is approximately 13 km from the Qitianling granite complex, and thus far, no magmatic intrusion has been found in this coalmine. However, some mineral veinlets (e.g., calcite, illite) can be found in the coal seams and their host rocks from the coal working faces. The Longtan Formation is its major coal-bearing formation [24,29]. Based on their lithological compositions, four separate intervals can be identified: a non-coal-bearing interval, a lower coal-bearing interval, a marine layer interval, and an upper coal-bearing interval from bottom to top (Figure 2) [29]. Coal seams with economic value are located in the lower coal-bearing interval.

The thickness of the lower coal-bearing interval varies from 64.0 to 278.3 m (average 129.8 m), and it mainly consists of fine-medium sandstone, siltstone, silty mudstone, and coal seams, which are a set of clastic rocks of the marine-terrestrial transitional facies [29]. The lower coal-bearing interval contains No. 13, 12L, 12U, 11, 10, 9, and 2 coal beds from bottom to top, of which 12U and 12L Coals are minable. Both 12U and 12L Coals from the Meitian Mine vary from less than 0.5 m to 5 m thick. The study area has been subjected to several tectonic events since the coal-forming period [24], resulting in the destruction of coal structure at different degrees and the impairment of coal permeability. Unlike other coalmines in the Meitian Coalfield, the gas content of the studied coal seams is very low.

The non-coal-bearing interval, which is more than 100 m thick on average, is mainly composed of fine-medium sandstone with interbeds of sandy mudstone and siltstone (Figure 2). The marine bed interval mainly consists of sandy mudstone, mudstone, siltstone, and limestone, with an average thickness of more than 200 m (Figure 2). The upper coal-bearing interval comprises mudstone interlayered with thin fine-grained sandstone, siltstone, and non-minable coal seams, which are not shown in Figure 2.

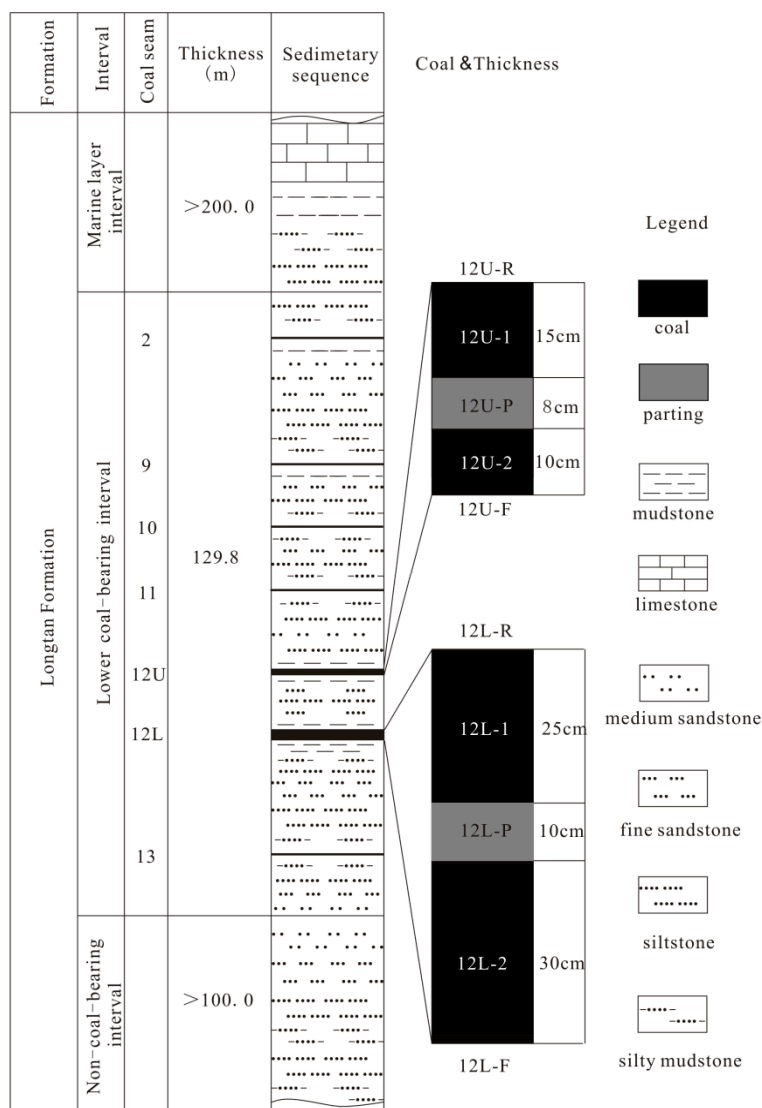


Figure 2. Sedimentary sequences of the Meitian Mine and bench samples used in this study.

3. Material and Analytical Methods

The samples, including coals, partings, roofs, and floors, were collected from the coal working faces in Meitian Mine, whose burial depth are about 300 m. Ten bench samples were collected in total, including four coal samples, two partings, two roofs, and two floors, and numbered as indicated in Figure 2. Each coal bench sample was cut over an area 10 cm wide and 10 cm deep. Samples were immediately sealed and stored in plastic bags after they were collected to minimize contamination and oxidation. The texture properties of the studied coals are dominated by granulated coal, followed by cataclastic coal, and even undeformed coal with banded structure.

The proximate analysis for all the coal bench samples was conducted according to ASTM Standards D3173-11 (2011) [30], D3174-11 (2011) [31], and D3175-11 (2011) [32]. Based on ASTM Standard D3177-02 (2002) [33], the total sulfur content was analyzed. Random vitrinite reflectance (R_o , r_{an}) was measured using a Leica DM2500P reflected light microscope (Leica, Wetzlar, Germany) following ASTM D2798-05 (ASTM Standards D2798-05, 2005) [34].

A D/max-2500/PC powder diffractometer (Rigaku Corporation, Tokyo, Japan) was used to conduct X-ray powder diffraction (XRD) analysis to determine the mineral compositions of the samples. The sample preparation, experiment conditions, and experiment procedure for XRD analysis are as described by Dai et al. (2017) [5]. Each XRD pattern was recorded over a 2θ interval of 2.6° – 70° ,

with a step size of 0.01° . Prior to XRD analysis, the powdered coal samples were transformed to ash at low-temperatures ($<150^\circ\text{C}$) using an EMITECH K1050X Plasma Asher (Quorum Technologies, Lewes, UK). In addition, a field emission-scanning electron microscope in conjunction with an energy-dispersive X-ray spectrometer (FESEM-EDS) was used to further determine the mineral compositions of the bench samples. The experiment conditions and experiment procedure are generally as described in Dai et al. (2017) [5]. The samples were coated gold for low-vacuum SEM working conditions. The working distance of the FESEM-EDS was 10 mm, the beam voltage was 15 or 20 kV, the aperture was 6, and the spot size was 4 or 5.

To conduct geochemical analysis, all the samples were crushed and ground to pass through 200 mesh ($75\ \mu\text{m}$). X-ray fluorescence spectrometry (XRF) was used to determine the oxide concentration of major elements (i.e., SiO_2 , TiO_2 , Al_2O_3 , Fe_2O_3 , MgO , CaO , Na_2O , K_2O , and P_2O_5) in samples. Prior to XRF analysis, both coal samples and non-coal samples were ashed 815°C . Barring a few elements (i.e., As, Se, Hg, F, Re, and B), concentrations of the trace elements in the coal and non-coal samples were determined by quadrupole inductively coupled plasma mass spectrometry (ELAN DRE-e Q-ICP-MS, Waltham, MA, USA). The experiment procedure for the ICP-MS analysis was mainly conducted in accordance with the methods reported in Han et al. (2015) [35]. A 50-mg powder sample was dissolved in a high-pressure Teflon bomb with 1 mL HF and 2 mL HNO_3 at 190°C for 48 h. After removing HF by heating, the residue was dissolved in 2 mL H_2O and 2 mL HNO_3 with an appropriate amount of Rh at 145°C for 12 h. Rh was used as an internal standard to monitor instrument drift during the analysis.

4. Results

4.1. Coal Chemistry and Vitrinite Reflectance

The proximate analysis and total sulfur of the bench samples of 12U and 12L Coals from the Meitian Mine are shown in Table 1. The mean sulfur content in 12U and 12L Coals is 0.41% and 0.58%, respectively (Table 1), indicating that they are classified as low sulfur coals [36]. The average volatile matter yields of 12U and 12L Coals are 9.67% and 7.41% (Table 1), respectively, and the average vitrinite reflectance values of 12U and 12L Coals are 2.80% and 3.17%, respectively, indicating that the Coals are low volatile anthracite coals according to ASTM D388-12(2012) [37]. The ash yields of 12U and 12L Coals shown in Table 1 are 10.26% and 45.47%, respectively, and they are classified accordingly as low- and high-ash coal according to Chinese Standard GB/T 15224.1-2010 [38].

Table 1. Proximate analysis (%) and vitrinite reflectance (%) of coal benches in the Meitian Mine.

Coal Seam	Sample No.	Thickness (cm)	M_{ad}	A_d	V_{daf}	$S_{t,d}$	$R_{o,ran} \pm S_{tdev}$
12U	12U-1	15	2.58	7.07	11.18	0.38	2.64 ± 0.35
	12U-2	10	4.82	13.44	8.15	0.43	2.96 ± 0.24
12L	12L-1	25	2.39	46.80	8.19	0.64	2.89 ± 0.41
	12L-2	30	6.13	44.14	6.62	0.52	3.45 ± 0.16
12U	Av	12.5	3.70	10.26	9.67	0.41	2.80 ± 0.23
12L	Av	27.5	4.26	45.47	7.41	0.58	3.17 ± 0.46

M, moisture; A, ash yield; V, volatile matter; S_t , total sulfur; ad, as-received basis; d, dry basis; daf, dry and ash-free basis; $R_{o,ran}$, random vitrinite reflectance; Av, average; S_{tdev} , standard deviation.

4.2. Geochemistry

4.2.1. Major Element Oxides

The percentage of major-element oxides in the Meitian coal bench samples and host rocks, are shown in Table 2. It can be seen that the concentrations of the major-element oxides in both 12U Coal and 12L Coal are much higher than common Chinese coals [1]. Compared with 12U Coal,

the percentage of major-element oxides in 12L Coal is much higher. From Table 2, it can be also seen that the percentage of each major element oxide in the Meitian coal bench samples is higher than the average values for Chinese coals reported by Dai et al. (2012) [1], especially K_2O . Compared with 12U Coal, 12L Coal contains higher proportions of SiO_2 , Al_2O_3 , TiO_2 , Na_2O , MgO , and K_2O in particular, and lower concentrations of Fe_2O_3 , CaO , and P_2O_5 .

Table 2. Loss on ignition (LOI, %), and percentage of major oxide elements in samples from the Meitian Mine (%).

Sample No.	LOI	SiO_2	TiO_2	Al_2O_3	Fe_2O_3	MgO	CaO	Na_2O	K_2O	P_2O_5	SiO_2/Al_2O_3
12U-R	28.71	59.75	0.94	15.02	10.17	0.69	2.35	0.50	1.86	0.28	3.98
12U-1	92.96	36.82	1.06	11.89	23.84	0.76	3.89	0.51	0.98	0.36	3.10
12U-P	30.52	68.28	1.08	21.41	2.60	0.62	2.40	0.50	2.81	0.35	3.19
12U-2	86.60	36.76	0.80	13.26	21.97	0.57	1.45	0.50	1.31	0.44	2.77
12U-F	19.89	67.96	0.80	12.00	4.89	0.74	4.24	0.49	1.86	0.31	5.66
12U-WA	90.42	36.80	0.96	12.44	23.09	0.68	2.91	0.51	1.11	0.39	2.96
12L-R	24.12	66.43	1.05	25.68	3.72	1.04	0.70	0.50	3.67	0.35	2.59
12L-1	53.27	54.94	1.17	30.58	7.83	0.95	1.01	0.52	4.17	0.40	1.80
12L-P	23.85	66.29	1.15	24.54	2.56	0.72	0.85	0.51	3.72	0.34	2.70
12L-2	55.90	57.28	1.27	31.86	5.54	1.16	1.29	0.53	4.43	0.37	1.80
12L-F	26.12	66.13	1.14	26.69	2.35	1.08	1.00	0.51	3.94	0.36	2.48
12L-WA	54.70	56.22	1.22	31.28	6.58	1.06	1.16	0.53	4.31	0.38	1.80
China ^a	n.d.	8.47	0.33	5.98	4.85	0.22	1.23	0.16	0.19	0.09	1.42

WA, weight average for coal bench samples of seam section; n.d., no data; ^a Average concentrations of elements in common Chinese coals [1].

4.2.2. Trace Elements

The concentrations of trace elements detected in coals are presented in Table 3. It can be seen that Pb is significant enriched in the 12U Coal ($94.72 \mu\text{g/g}$; $cc > 10$) (Figure 3a) according to the enrichment classification proposed by Dai et al. (2015) [39]. Moreover, Zn ($101.76 \mu\text{g/g}$), Sn ($4.29 \mu\text{g/g}$), and Cd ($0.62 \mu\text{g/g}$) are slightly enriched, with $2 < cc < 5$ (Figure 3a). In contrast to 12U Coal, W ($10.06 \mu\text{g/g}$), Rb ($234.36 \mu\text{g/g}$), and Cs ($26.10 \mu\text{g/g}$) are significantly enriched in 12L Coal, with $10 < cc < 100$ (Figure 3b), and Th, V, Zn, and Zr are enriched ($5 < cc < 10$) (Figure 3). The rest of the elements are either slightly enriched ($2 < cc < 5$) or close to the global averages for hard coals ($0.5 < cc < 2$) with the exception of Ge, As, Sr, Mo, Sb, and Bi. The trace element data show that the host rocks are rich in W, Rb, Cs, Be, Th, Ta, Rr, and Ho, but especially W, Rb, and Cs (Figure 3c), when compared with the global average for mudstones [40].

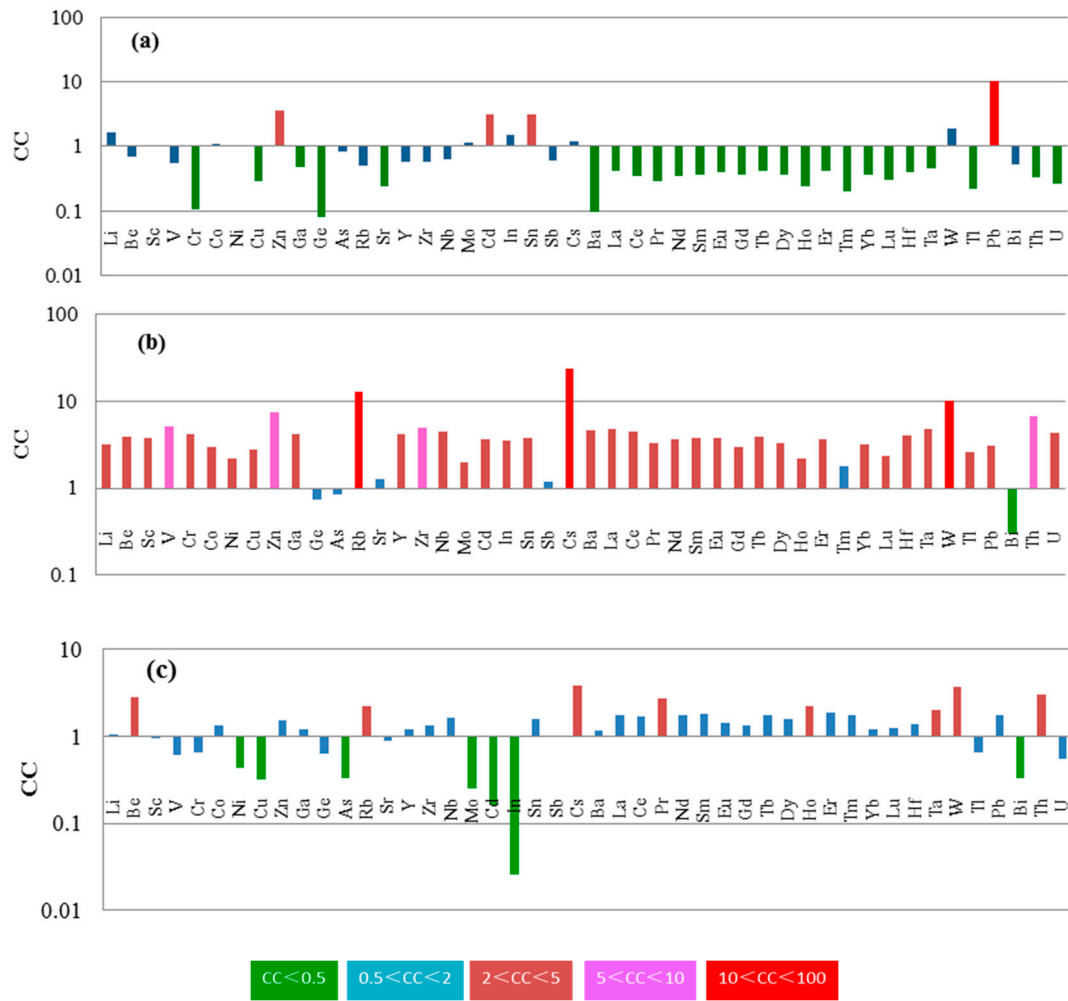


Figure 3. Concentration coefficients (CC) of trace elements in 12U Coal (a), 12L Coal (b), and host rocks (c) from the Meitian Mine, normalized by global average trace element concentrations in hard coals and average mudstones [40].

Table 3. Concentrations of trace elements in coals and host rocks from the Meitian Mine ($\mu\text{g/g}$).

Element	12U Beaches						12L Beaches						World
	12U-R	12U-1	12U-P	12U-2	12U-F	12U-WA	12L-R	12L-1	12L-P	12L-2	12L-F	12L-WA	
Li	33	17	31	33	51	23	103	59	29	33	34	45	14
Be	4.9	0.81	5.2	2.2	9.1	1.4	7.4	8.9	7.2	6.8	6.7	7.8	2.0
Sc	14	bdl	4.3	bdl	15	bdl	16	14	14	14	14	14	3.7
V	144	16	57	16	134	16	123	131	141	153	126	143	28
Cr	69	1.0	29	2.9	78	1.8	75	72	70	70	66	71	17
Co	17	1.2	15	14	29	6.5	21	16	26	20	28	18	6.0
Ni	37	15	22	20	37	17	26	37	50	37	43	37	17
Cu	40	3.8	5.8	5.9	9.8	4.7	55	47	40	41	44	44	16
Zn	122	100	59	105	84	102	379	196	247	218	412	208	28
Ga	25	2.1	12	4.1	26	2.9	27	25	28	26	25	25	6.0
Ge	1.7	0.12	0.87	0.30	2.0	0.19	2.4	1.7	1.7	1.9	2.0	1.8	2.4
As	7.4	1.5	14	15	20	6.9	2.8	5.6	3.5	8.0	4.3	6.9	8.3
Rb	235	4.8	111	16	256	9.1	184	242	221	228	225	234	18
Sr	141	20	124	29	254	24	230	145	125	116	208	129	100
Y	35	5.2	18	4.4	42	4.9	40	39	39	32	37	35	8.4
Zr	169	22	102	20	274	21	243	174	212	186	187	181	36
Nb	17	2.9	11	2.0	27	2.5	24	18	21	18	20	18	4.0
Mo	5.6	2.8	2.8	1.8	4.9	2.4	4.0	6.7	3.8	2.2	5.9	4.2	2.1
Cd	0.40	0.42	0.55	0.91	0.72	0.62	1.1	0.59	0.98	0.84	1.4	0.73	0.20
In	0.11	0.03	0.08	0.10	0.16	0.06	0.11	0.15	0.13	0.13	0.11	0.14	0.04
Sn	5.1	0.20	11	10	23	4.3	11	5.0	6.2	5.4	5.4	5.2	1.4
Sb	7.4	0.53	1.6	0.73	6.0	0.61	3.7	1.9	0.82	0.58	1.7	1.2	1.0
Cs	15	0.67	18	2.3	32	1.3	25	29	22	24	23	26	1.1
Ba	770	10	304	21	722	14	543	682	766	696	788	690	150
La	53	5.3	29	3.2	68	4.5	60	55	57	52	55	53	11
Ce	101	9.2	53	6.2	128	8.0	118	106	111	101	109	103	23
Pr	11	1.1	5.6	0.73	14	0.97	13	12	12	11	12	11	3.4
Nd	45	4.9	21	2.9	52	4.1	51	46	47	43	47	44	12
Sm	8.2	0.94	3.7	0.61	9.8	0.81	9.5	8.9	8.7	7.9	8.4	8.3	2.2
Eu	1.8	0.21	0.68	0.11	1.7	0.17	2.0	1.8	1.7	1.5	1.7	1.6	0.43
Gd	7.1	1.2	3.4	0.74	8.5	1.0	8.5	9.5	8.0	6.8	8.1	8.0	2.7
Tb	1.0	0.15	0.52	0.10	1.3	0.13	1.2	1.4	1.2	1.1	1.1	1.2	0.31
Dy	6.0	0.85	3.1	0.61	7.4	0.75	7.0	7.7	7.0	6.1	6.7	6.8	2.1
Ho	1.3	0.15	0.62	0.13	1.5	0.14	1.4	1.4	1.4	1.2	1.4	1.3	0.57

Table 3. Cont.

Element	12U Beaches						12L Beaches						World
	12U-R	12U-1	12U-P	12U-2	12U-F	12U-WA	12L-R	12L-1	12L-P	12L-2	12L-F	12L-WA	
Er	3.9	0.40	2.0	0.42	4.6	0.41	4.2	4.0	4.1	3.4	3.9	3.7	1.0
Tm	0.56	0.06	0.27	0.06	0.63	0.06	0.60	0.56	0.56	0.50	0.52	0.53	0.30
Yb	3.7	0.34	1.9	0.39	4.3	0.36	4.0	3.5	3.6	3.0	3.6	3.2	1.0
Lu	0.53	0.06	0.28	0.06	0.62	0.06	0.57	0.50	0.53	0.44	0.50	0.47	0.20
Hf	4.7	0.46	2.7	0.50	7.5	0.48	6.8	4.9	5.3	4.8	5.0	4.9	1.2
Ta	1.4	0.17	0.87	0.10	2.2	0.14	2.1	1.5	1.7	1.4	1.7	1.5	0.30
W	11	2.3	5.1	1.1	12	1.8	8.0	9.4	9.2	11	8.6	10	0.99
Tl	3.7	0.12	0.64	0.15	1.5	0.13	1.1	1.6	1.6	1.4	1.6	1.5	0.58
Pb	58	128	61	45	75	95	63	45	20	13	26	28	9.0
Bi	0.35	0.81	0.30	0.20	0.50	0.57	0.45	0.54	0.25	0.17	0.32	0.34	1.1
Th	22	1.1	10	0.96	29	1.1	27	22	24	22	23	22	3.2
U	13	0.51	3.4	0.50	7.9	0.51	7.4	11	6.7	6.0	7.3	8.1	1.9

World, world hard coals, data from Ketris and Yudovich (2009) [40]; bdl, below detection limit; WA, weighted average for coal bench samples of seam section (weighted by the thickness of sample interval).

4.2.3. Rare Earth Elements and Yttrium (REY)

In this study, threefold division (e.g., light, medium, and heavy fractions) of REY is adopted according to the classification of Seregin and Dai (2012) [6]. REY were normalized by the Upper Continental Crust (UCC) when La_N/Lu_N , La_N/Sm_N , Gd_N/Lu_N , and Y_N/Ho_N were calculated, and Eu/Eu^* , Ce/Ce^* , and Gd/Gd^* were calculated by the following formulae according to Bau and Dulski (1996) [41] and Dai et al. (2016, 2017) [5,42]. In Table 4, it can be seen that the concentrations of REY in 12U and 12L Coal are 26.33 and 282.17 $\mu\text{g/g}$, respectively, and the latter is much higher than that of global bituminous coal (68.6 $\mu\text{g/g}$) [40]. In addition, compared with 12U and 12L Coals, the partings, roofs, and floors have much higher average REY concentrations (Table 4).

$$Eu_N/Eu_N^* = Eu_N / [(Sm_N \times 0.67) + (Tb_N \times 0.33)] \quad (1)$$

$$Ce_N/Ce_N^* = Ce_N / (0.5La_N + 0.5Pr_N) \quad (2)$$

$$Gd_N/Gd_N^* = Gd_N / [(Sm_N \times 0.33) + (Tb_N \times 0.67)] \quad (3)$$

According to the classification of enrichment patterns of REY [6], with the exception of 12U-P and 12U-F samples (both L-enrichment types), the REY enrichment patterns in almost all coal benches, partings, roofs, and floors are M-type ($La_N/Sm_N < 1$, $Gd_N/Lu_N > 1$) and characterized by a negative Ce anomaly and positive Y and Gd anomalies (Table 4; Figure 4). Except for 12U-R, 12U-1, 12L-R, and 12L-F samples, the coal benches, partings, and host rocks generally exhibit negative or no Eu anomalies (Table 4; Figure 4).

Table 4. REY parameters of coals, partings, roofs, and floors from the Meitian Mine.

Sample No.	REY	LREY	MREY	HREY	La_N/Lu_N	La_N/Sm_N	Gd_N/Lu_N	Eu/Eu^*	Ce/Ce^*	Gd/Gd^*	Y_N/Ho_N
12U-R	279.48	218.39	51.12	9.97	1.07	0.97	1.13	1.16	0.94	1.13	1.01
12U-1	30.07	21.45	7.61	1.01	0.95	0.85	1.64	1.10	0.85	1.36	1.27
12U-P	142.67	111.88	25.79	5	1.10	1.16	1.03	0.94	0.94	1.10	1.06
12U-2	20.72	13.68	5.98	1.06	0.58	0.80	1.04	0.88	0.91	1.30	1.24
12U-F	344.03	271.69	60.73	11.61	1.18	1.05	1.16	0.91	0.95	1.10	1.00
12U-WA	26.33	18.34	6.96	1.03	0.80	0.83	1.40	1.03	0.87	1.35	1.28
12L-R	320.35	250.59	58.97	10.79	1.11	0.94	1.25	1.09	0.97	1.14	1.05
12L-1	296.59	227.4	59.28	9.91	1.17	0.92	1.59	1.00	0.95	1.18	1.03
12L-P	302.76	235.8	56.77	10.19	1.15	0.98	1.27	0.99	0.96	1.11	1.00
12L-2	270.37	214.82	47.07	8.48	1.27	0.99	1.29	1.00	0.96	1.07	1.00
12L-F	295.45	231.1	54.49	9.86	1.18	0.99	1.36	1.04	0.97	1.18	1.00
12L-WA	282.17	220.42	52.62	9.13	1.21	0.97	1.43	1.00	0.95	1.13	1.02
World	68.61	51.6	13.94	3.07	0.015	0.22	1.23	0.16	0.19	0.092	1.42

4.3. Minerals in the Coal

The mineralogical compositions in the low-temperature ash (LTAs) of 12U and 12L Coals are shown in Table 5 and Figure 5. The content of chlorite in 12U Coal was found to be highest and can be as high as 50.4%, with an average of 45.8%. The contents of quartz, calcite, plagioclase, I/S, and K-feldspar in 12U Coal decrease in sequence, with an average of 35.5%, 8.1%, 4.2%, 2.5%, and 2.2%, respectively. While the content of illite (average 36.7%) in 12L Coal is the highest, followed by quartz (average 27.7%), chlorite (average 15.3%), I/S (average 8.3%), Kaolinite (average 4.5%), plagioclase (average 3.1%), and K-feldspar (average 2.0%). In Table 5, it can be also seen that almost all partings, roofs, and floors have similar mineral compositions dominated by illite (average 45.3%) and quartz (average 45.3%) followed by chlorite (average 7.1%) and calcite (average 4.3%). Several other phases, including fluorite, dolomite, rutile, arsenopyrite, apatite, gypsum, tremolite, diopside, and talc are mainly identified in 12L Coals by SEM-EDS techniques (Figures 6–8), while marcasite in cockscomb form, clintheriform, and spear shapes (Figure 6f) is mainly identified in 12U Coal.

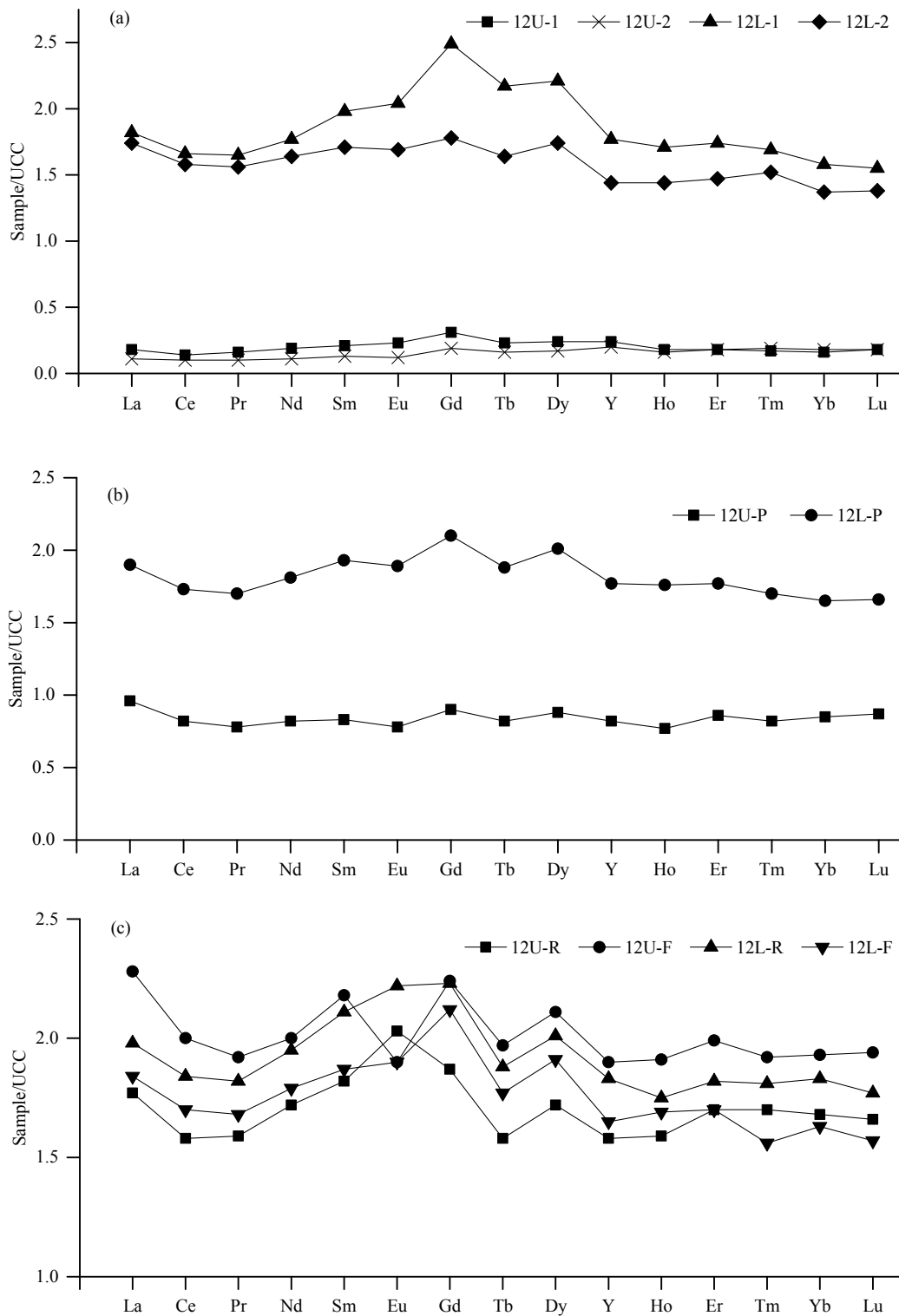


Figure 4. Distribution patterns of REY in coal benches (a), partings (b), and roofs and floors (c). REY are normalized by upper continental crust concentrations (UCC) [43].

Table 5. Mineral compositions (%) of low-temperature ash, partings, roofs, and floors determined by XRD and Siroquant techniques.

Sample No.	Quartz	K-Feldspar	Plagioclase	Calcite	Pyrite	Kaolinite	Illite	I/S	Chlorite
12U-R	39.0	0.5	4.1	3.2			45.8		7.4
12U-1	35.6	0.8	3.6	10.9			0.5		50.4
12U-P	39.7	0.9	4.9	2.5			46.8		5.2
12U-2	34.9	3.6	4.8	5.2			2.4	4.9	41.2
12U-F	48.6	0.2	4.1	7.3			26.7		13.1
12L-R	34.7	1.4	3.3				52.1		8.5
12L-1	26.8	2.0	2.0		0.6	8.9	31.6	16.5	11.7
12L-P	39.0	1.2	2.8		1.0		52.6		3.4
12L-2	28.5	1.9	4.2	4.9			41.7		18.8
12L-F	39.2	1.4	3.1	4.1			47.5		4.7

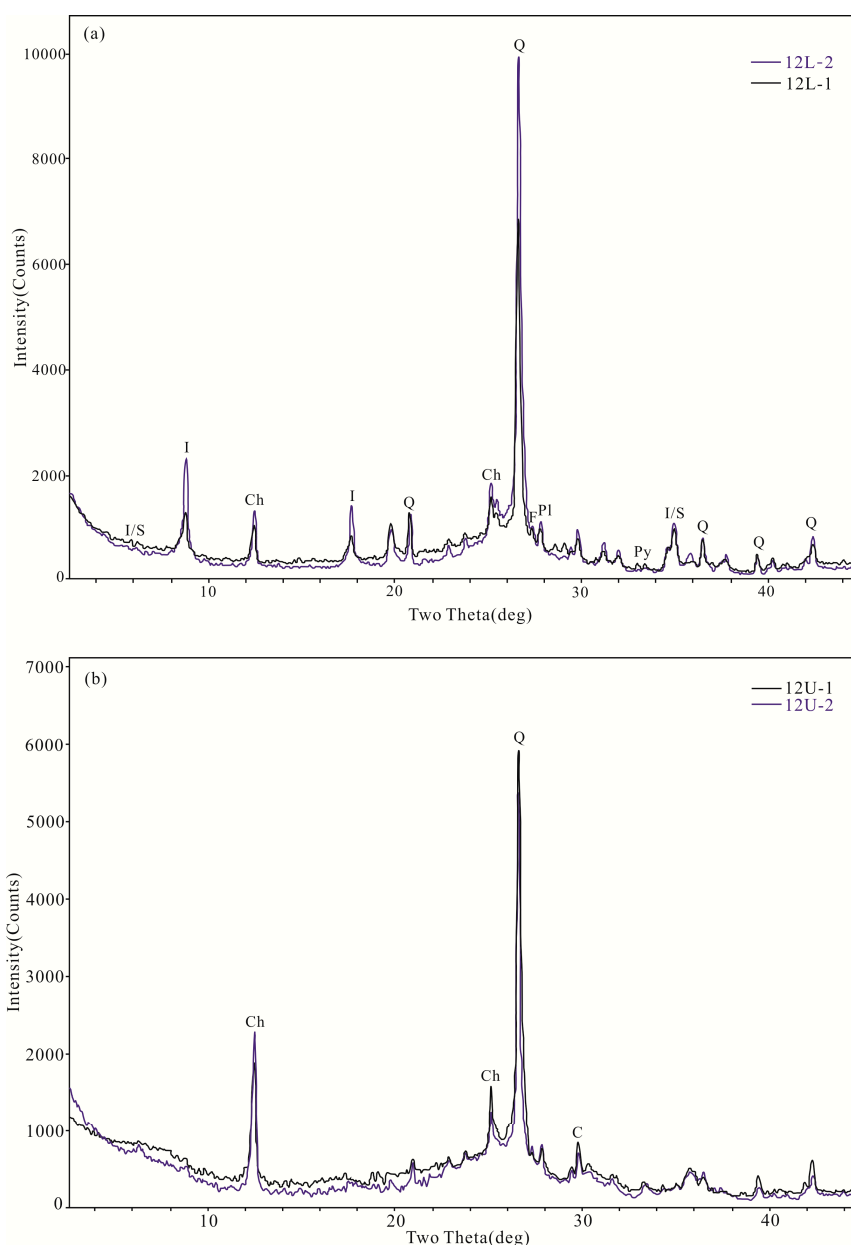


Figure 5. XRD patterns of 12L Coal (a) and 12U Coal (b). I = illite; Ch = chlorite; I/S = mixed-layer illite/smectite; Q = quartz; Pl = plagioclase; F = K-feldspar; C = calcite; Py = pyrite.

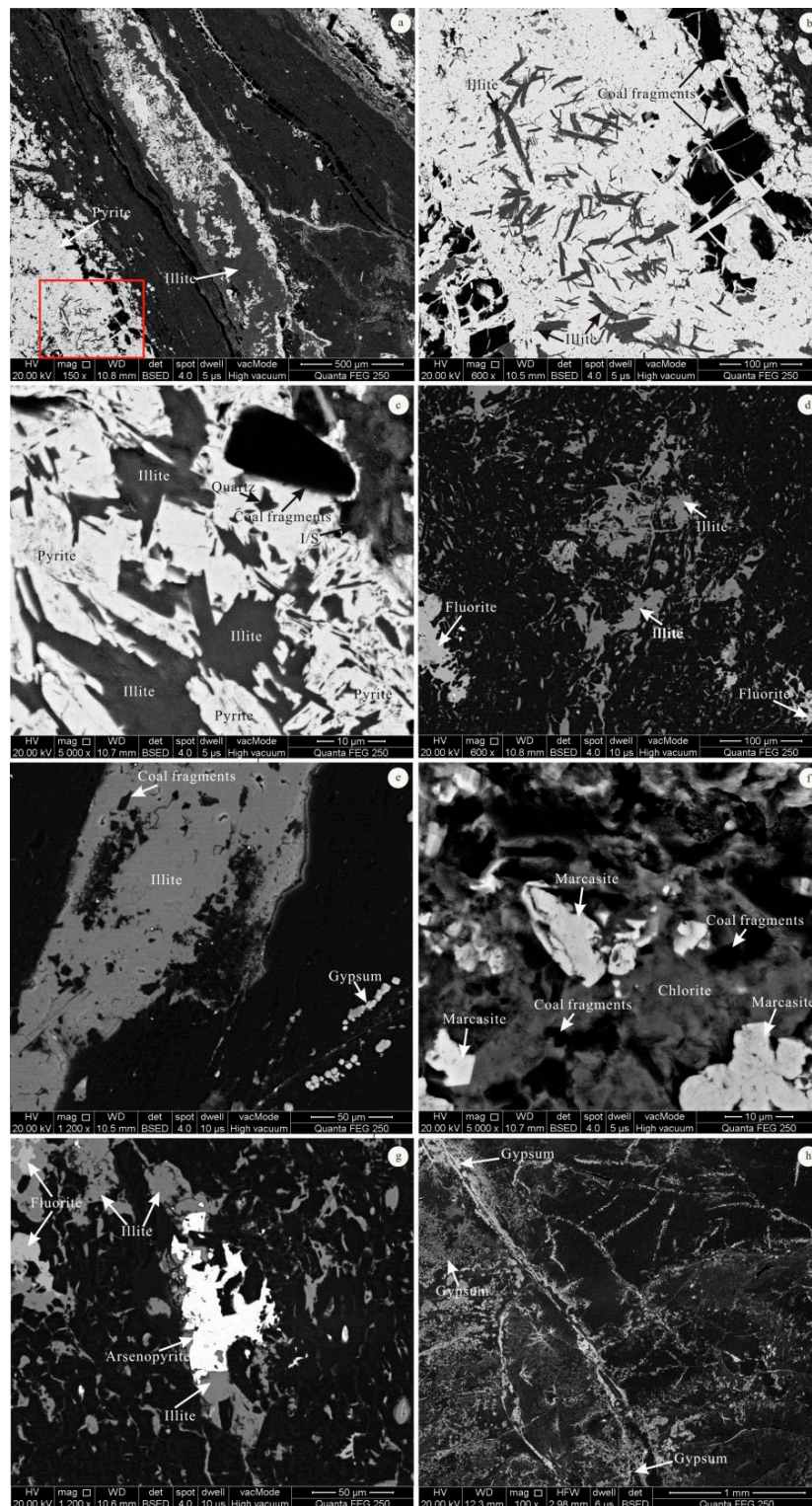


Figure 6. SEM back-scattered electron images of illite, chlorite, I/S, and pyrite in 12U and 12L Coals. (a) Fracture-filling pyrite and illite, and some illite and coal fragments distributed in the fracture-filling pyrite in sample 12L-1; (b) enlargement of the red square in (a); (c) fracture-filling pyrite and I/S, and some illite and coal fragments distributed in the pyrite in sample 12L-1; (d) vesicle-filling illite and fluorite in sample 12L-2; (e) fracture-filling illite in sample 12L-2; (f) vesicle- and fracture-filling chlorite, and some coal fragments and marcasite distributed in the chlorite in sample 12U-2; (g) vesicle- and fracture-filling illite and arsenopyrite and vesicle-filling fluorite and cavities of illite filled by fluorite in sample 12L-2; and (h) gypsum mainly distributed along fractures in sample 12L-2.

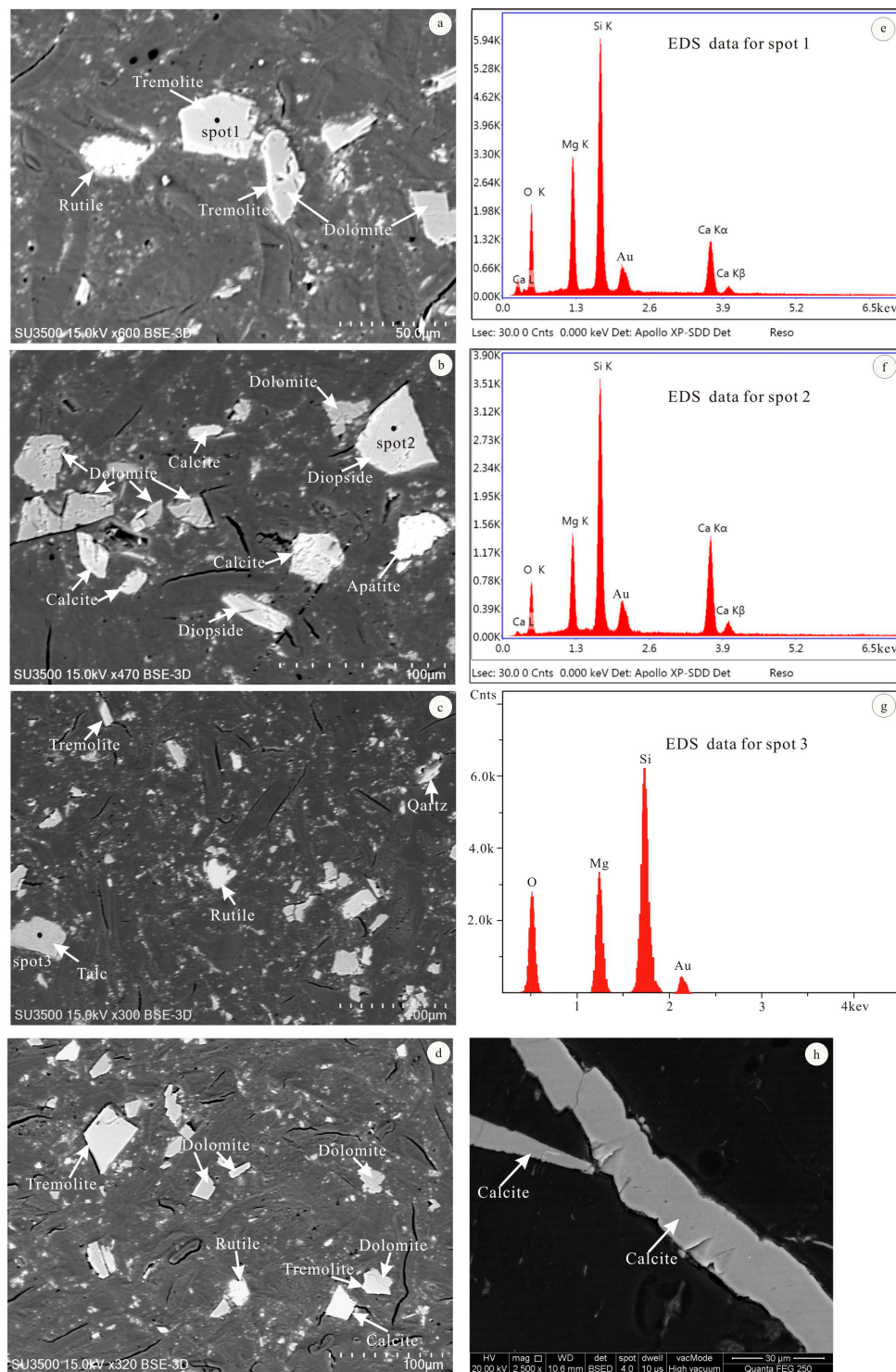


Figure 7. SEM back-scattered electron images of carbonate minerals, rutile, apatite, tremolite, diopside, and talc in 12U and 12L Coals. (a–d), cleat-filling calcite, dolomite, tremolite, diopside and talc in 12L Coal; (e–g) EDS data for tremolite, diopside, and talc; and (h) fracturing-filling calcite in sample 12U-1.

4.4. Modes of Occurrence of Minerals

The modes of occurrence of minerals are shown in Figures 6–8. It can be seen that illite, chlorite, I/S, and pyrite in 12U and 12L Coals generally occur as vesicle- and fracture-filling minerals (Figure 6a–g), and coal fragments are typically distributed in these minerals (Figure 6a–c,e,f). Quartz in the coals mainly occurs as cavity fillings in other minerals (e.g., pyrite; Figure 6c) and discrete particles in the

organic matter (Figure 7c). Fluorite in 12L Coal mainly has three modes of occurrence, including vesicle- and fracture-filling in the organic matter (Figure 6d,g) and cavity-filling in illite (Figure 6g). Gypsum identified in 12L Coal is mainly distributed along fractures (Figure 6h).

Calcite, dolomite, apatite, tremolite, diopside, and talc identified by SEM-EDS generally occur as cleat fillings in the coals, especially in 12L Coal (Figure 7). Some dolomite is corroded and replaced by silicate minerals, such as tremolite (Figure 7a,d). The similar distribution of C, O, Ca, Mg, Si, and P indicate the possible occurrence of calcite, dolomite, apatite, and diopside in the 12L Coal (Figure 8). According to the grayscale on the BSE images, apatite generally shows the highest brightness of these minerals, followed by calcite, tremolite, and diopside (Figure 7b), whereas dolomite tends to have the lowest brightness (Figure 7a,b,d). For the partings, large proportions of illite, chlorite, and pyrite mainly occur as cavity and fracture fillings (Figure 9), and some coal fragments are also distributed in these minerals, especially in illite (Figure 9a–c,e).

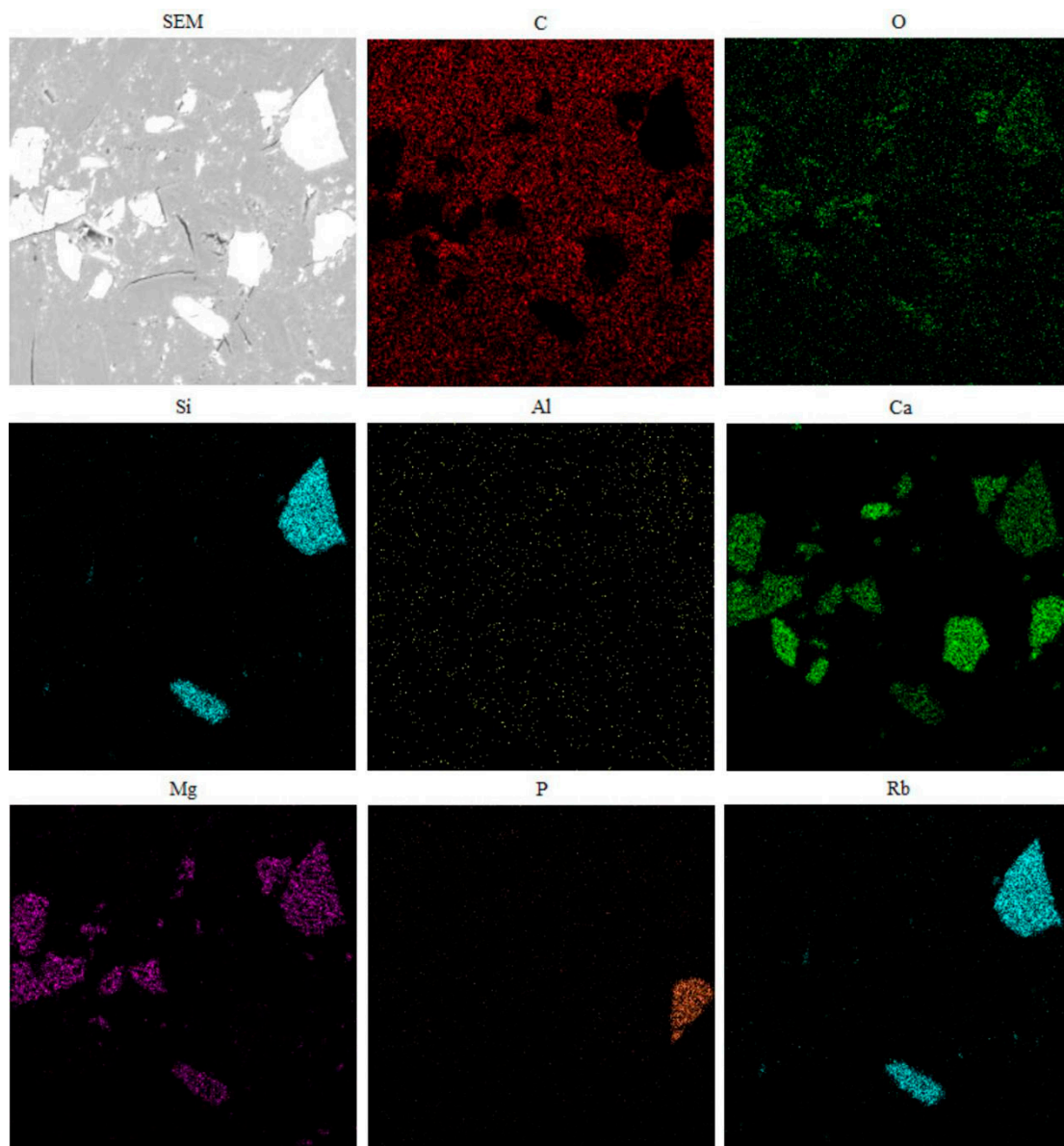


Figure 8. Areal distributions of C, O, Si, Al, Ca, Mg, P, and Rb in Figure 7b.

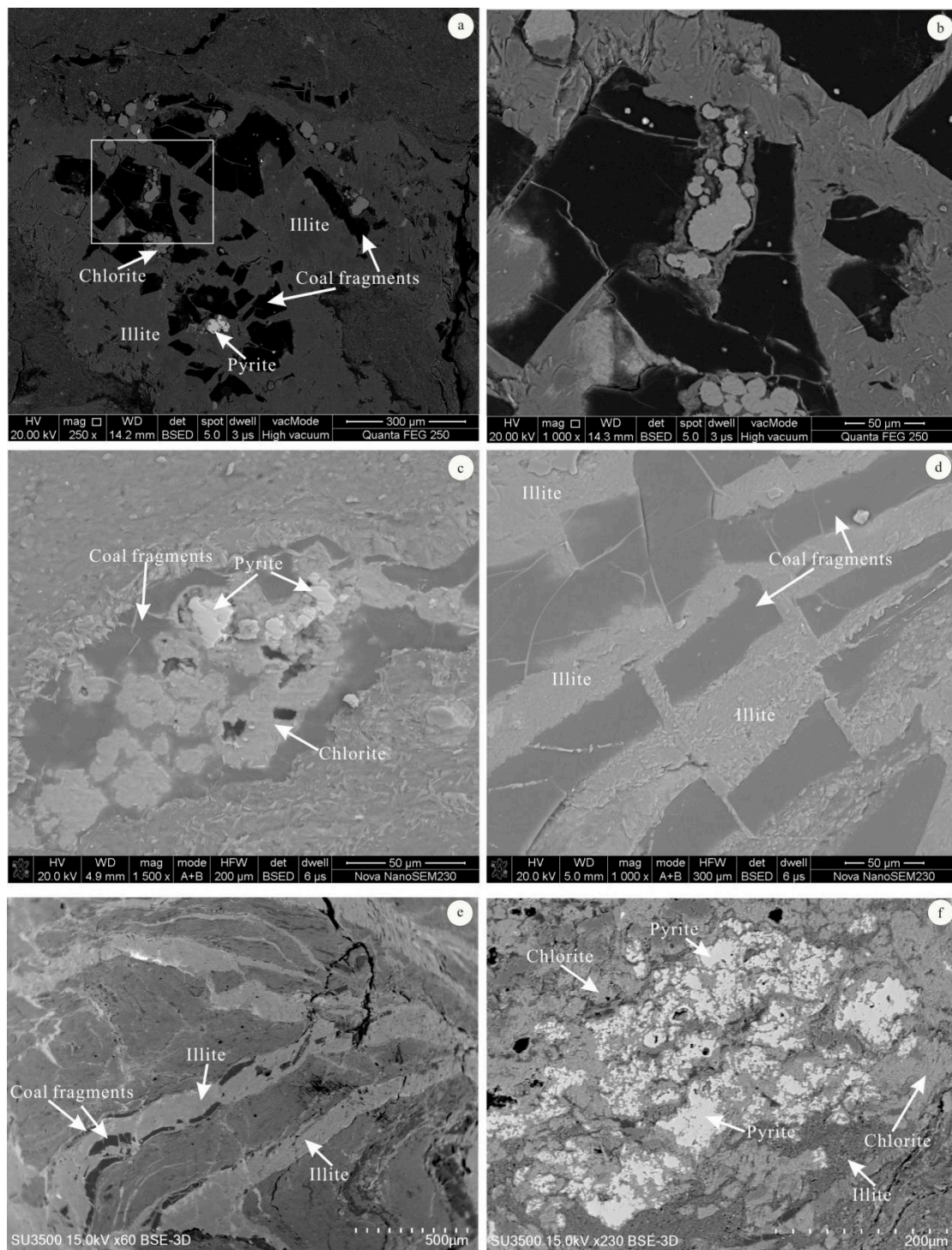


Figure 9. SEM and back-scattered electron images of minerals in partings. (a) Fracture-filling illite and some chlorite, pyrite, and coal fragments distributed in the illite in sample 12U-P; (b) enlargement of the white square in (a); (c) fracture-filling chlorite and coal fragments in sample 12U-P; (d) fracture-filling illite and coal fragments in sample 12L-P; (e) fracture-filling illite and coal fragments in sample 12L-P; (f) fracture-filling illite, chlorite, and pyrite in sample 12L-P.

5. Discussion

5.1. Enrichment Origin of Elements in the Coal: Magmatic Hydrothermal Fluids

In Table 1, it can be seen that the decreasing trend of vitrinite reflectance and increasing trend of volatile matter from the bottom to the top in this zone, is best explained by igneous intrusions. SEM-EDX results showed that vesicles and fractures in the coals and partings are well developed (Figures 6, 7 and 9) under the abnormal thermal metamorphism resulting from the intrusion of a Jurassic granitic pluton (the Qitianling granite complex). Moreover, they are almost filled by hydrothermal minerals (e.g., illite, pyrite, and fluorite). Such modes of crystallization in coal are generally related to the influence of magmatic hydrothermal fluids [22,44,45].

REY plots are similar for almost all coal bench samples, partings, roofs, and floors, showing an M-type REY distribution, Gd-maximum, and positive Y anomalies (Figure 4 and Table 4), which is likely connected with acid hydrothermal circulation [5,6,42,46]. The ascent of hydrothermal fluids under high pressure is also identified by the decreasing concentrations of most elements (e.g., W, Rb, Cs, V, Ni, and Zn; Table 3) from the bottom to the top of this zone [47,48], especially considering the similar zonal distribution of these elements in the host rocks (Table 3). Eskenazy (1982) [47] pointed out that coal deposits enriched in tungsten may be expected in rocks consisting of acid granitoids with high tungsten contents; the Qitianling granite complex in the north of the study area is one such granitoid that is significantly enriched in W, Rb, and Cs [49,50]. All these findings indicate that the enrichment of some elements, especially W, Rb, and Cs, in the coals of Meitian Mine is genetically associated with magmatic hydrothermal fluids.

5.2. Minerals Originating from Magmatic Hydrothermal Fluids

As shown in Figure 6, the clay minerals in 12U and 12L Coals, especially illite and chlorite, mainly occur as vesicle and fracture fillings, indicating that they originated from epigenetic magmatic hydrothermal fluids. In addition, some coal fragments are distributed within illite and chlorite (Figure 6e,f), further confirming their epigenetic origin. Pyrite is also very common in coals intruded by magmatic rocks [10,19,22,51]. The 12U and 12L Coals may have a very low pyrite content if there are no igneous intrusions, because the coal seams formed in a fluvial plain and were not influenced by sea water during peat accumulation [29]. SEM-EDX results showed that pyrite in the coals, especially 12L Coal, occurs as fracture or vesicle fill (Figure 6a–c,f), also indicating that it originated from epigenetic magmatic hydrothermal fluids [22,44,45,52].

Fluorite has been found in some coals, such as Heshan and Yishan coals in Guangxi province, southern China [53,54] and in Bulgarian coals [55]. Fluorite in the studied coals mainly occur as cavity-, vesicle-, and fracture-fillings (Figure 6d,g), indicating an epigenetic hydrothermal origin. It was reported that vesicle- and vein-filling carbonate minerals in coals intruded by magmatic rocks are very common [10,19,21,22,51]. Calcite and dolomite in the 12U and 12L Coals mainly occur as cleat and fracture fillings (Figure 7a,b,d,h), indicating an epigenetic hydrothermal origin. The formation of calcite and dolomite in the 12U and 12L Coals may be attributed to CO₂ from volatile matter in the intrusions [27,28,55], and to CO₂ sourced from reactions between thermally altered coals and materials from the intrusion, considering the carbon component in coals [9,10].

Tremolite, diopside, and talc are uncommon in other coals, even in thermally altered coals. In this study, these minerals generally occur as cleat fillings (Figures 7 and 8); some of them are distributed along the edge of the corroded dolomite (Figure 7a,d) and even occur as cavity-fill in the dolomite (Figure 7d), indicating an epigenetic hydrothermal origin. According to the relationship between these minerals and dolomite, they were probably formed from the reaction between dolomite and Si-rich magmatic hydrothermal fluids. Pei et al. (2011) [56] reported that tremolite, diopside, and talc can be formed from the metasomatic alteration of dolomitic marble and siliceous magmatic hydrothermal fluids, which may confirm this conclusion.

5.3. Mode of Occurrence of Rb, Cs, W, Pb, Zn and Cd

Seredin and Finkelman (2008) [4] have shown that “Metalliferous coal” is typically applied to coals with unusually high concentrations of potentially valuable trace elements (e.g., W, Cs, and Mo), at least ten times higher than the respective averages for the same elements in world coals. Furthermore, W and Cs in coals are typical rare metals and are considered promising for use [8]. The concentrations of Rb, Cs, and W in 12L Coal are more than ten times than that of world coals (Figure 3 and Table 3), which means they have potential for economic by-product recovery. On the other hand, high concentrations of toxic trace elements (i.e., Pb, Zn, and Cd) in the studied coals may result in adverse effects on human health and environments [8,57].

5.3.1. Rubidium

The rubidium concentration in 12L Coal is 234.36 $\mu\text{g/g}$ (Table 3), which is higher than that in global hard coals (average 18 $\mu\text{g/g}$) [40]. Furthermore, elevated Rb is not only found in the coal but in the host rock (Table 3), indicating that it has important economic significance for coal recovery. Although no one has set the exact and affirmative cut-off grades of Rb in coals up to now, it was proposed that if the concentration of Rb is 5 times higher than that the average of world coal [3,58]. It is generally believed that Rb in coal has an inorganic affinity; it mainly occurs in illite and mixed-layer clays and can readily substitute for potassium [3,57,59,60]. Our study results showed that rubidium in the coal is clearly associated with K-rich clay minerals (i.e., illite + I/S; Figures 8 and 10–12). From Figure 11, it is also clear that samples with higher Rb concentrations generally have higher K_2O contents, which might also confirm that the K-rich clay minerals (i.e., illite and I/S) are the main carriers of rubidium. Judging from 12L Coal, the content of illite and I/S in 12L-1 Coal is higher than that in 12L-2 Coal, resulting in higher concentration of Rb in 12L-1 Coal. Furthermore, as shown in Figures 8 and 10, Rb in the coals can also occur in other hydrothermal silicate minerals (i.e., tremolite, diopside, and talc). The high proportion of nitric acid and HF soluble rubidium reported by Finkelman et al. (2018) [57] may further verify this conclusion.

5.3.2. Cesium

The cesium concentration in 12L Coal is 26.10 $\mu\text{g/g}$ (Table 3), which is higher than that in global hard coals (average 1.1 $\mu\text{g/g}$) [40]. Similar to rubidium, elevated cesium is also found in the host rocks, which can increase its potential economic significance. Like Rb, no one has set the exact and affirmative cut-off grades of Cs in coals, but it has been suggested that if the concentration of Cs is 5 times higher than that of the average of world coal [3,58]. Some study results have shown that cesium in coal generally occurs in K-bearing minerals [2,3,61,62]. In this study, the vertical variation of Rb and Cs in 12U and 12L Coals are almost identical (Figures 11 and 12), which may confirm the hypothesis that Rb and Cs in coal display very similar geochemical behavior and are likely to have similar modes of occurrence in the coal [57]. Our study revealed that samples with elevated Cs concentrations generally have higher K-bearing minerals and K_2O contents (Figures 11 and 12), further indicating that K-rich clay minerals are the main carriers of cesium in the coals. Unfortunately, the areal distribution of Cs (not shown in Figures 8 and 10) shown by the SEM images is not as ideal as that of Rb in the coals, which might be attributed to its relatively low concentration in K-rich clay minerals.

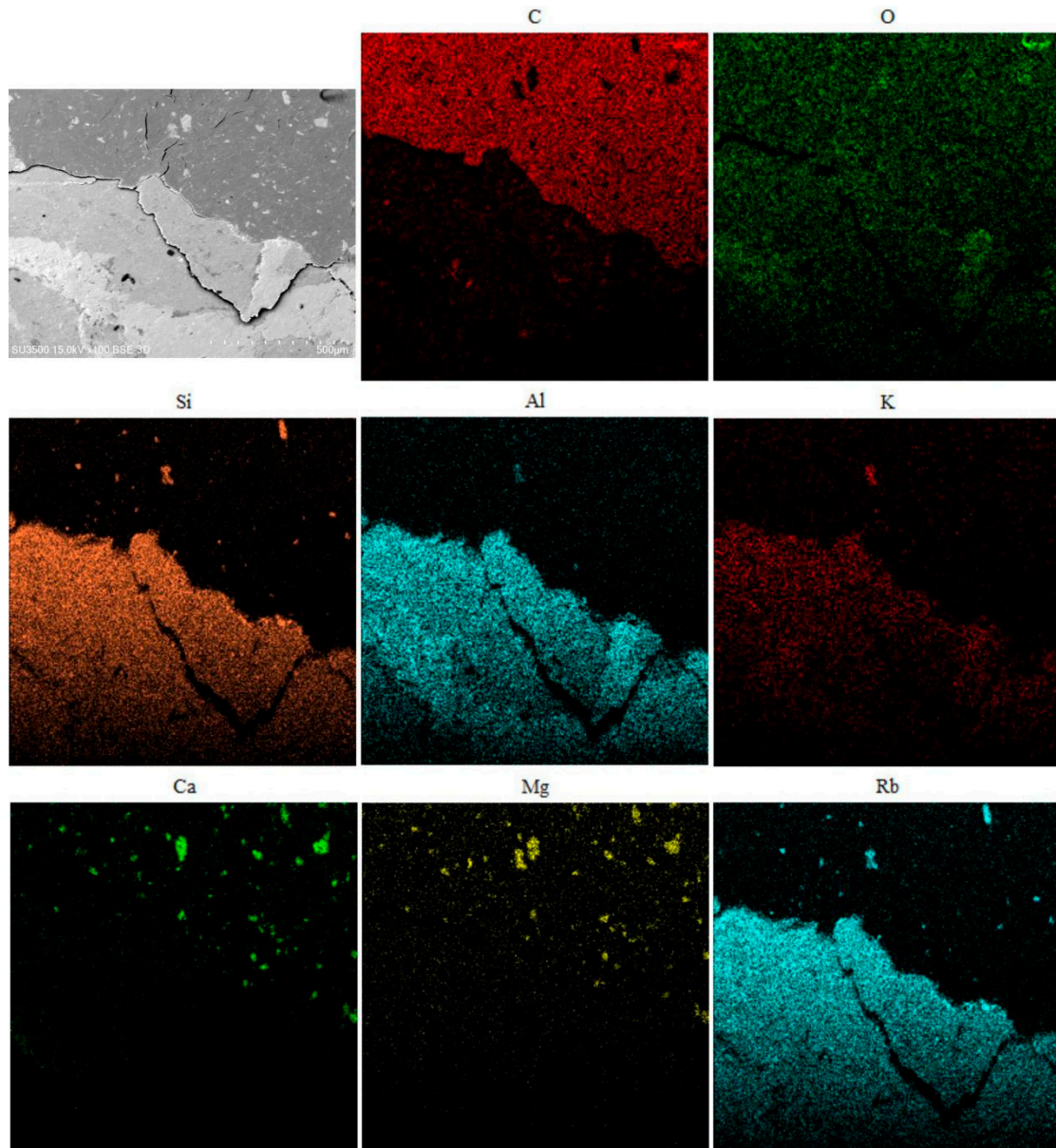


Figure 10. Areal distributions of C, O, Si, Al, K, Ca, Mg, Sn, Rb, CS, and W in sample 12L-2.

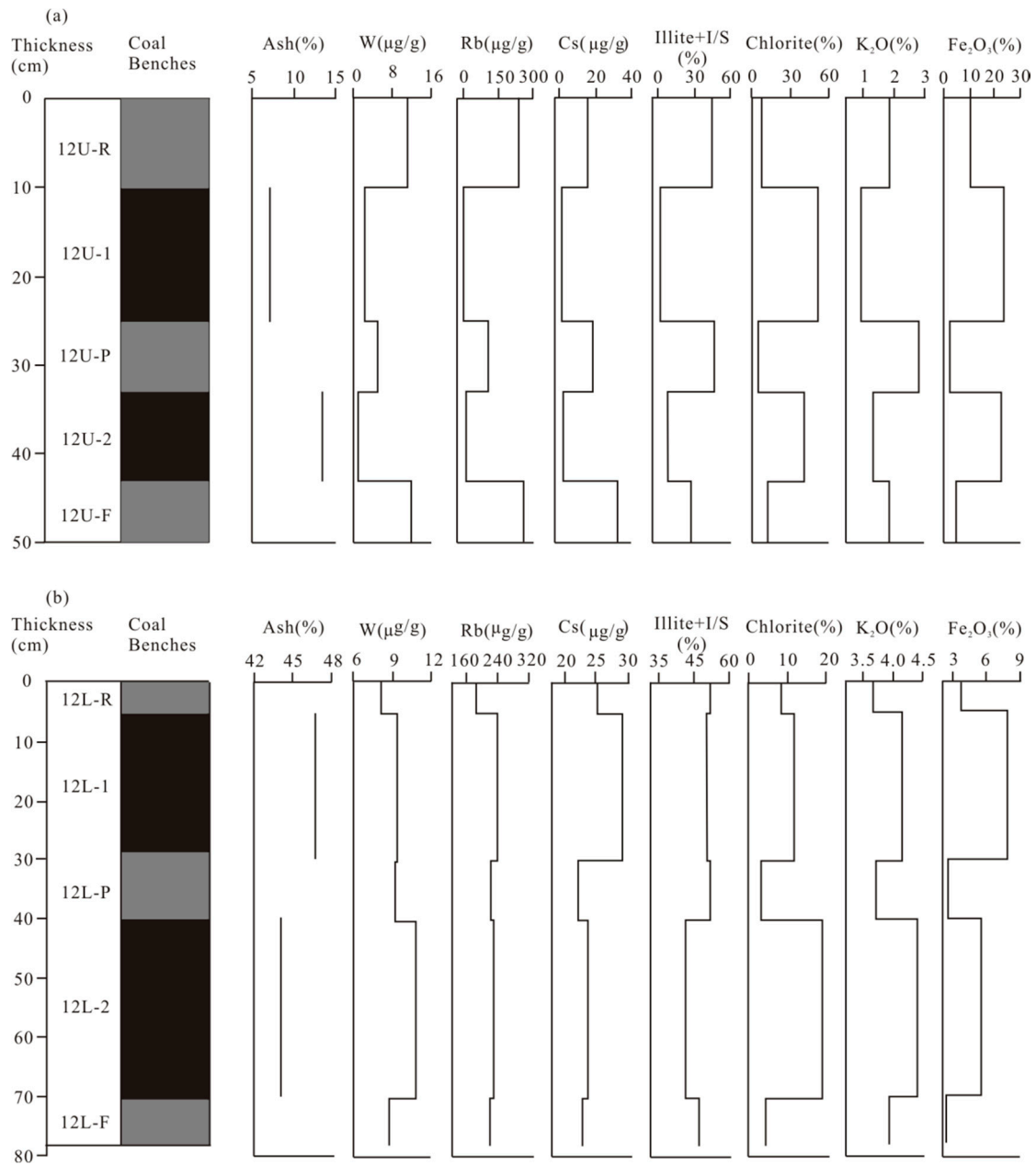


Figure 11. Vertical variations of W, Rb, Cs, illite + I/S, chlorite, K₂O, and Fe₂O₃ concentrations, as well as ash yield contents in the coal. (a) 12U Coal; (b) 12L Coal.

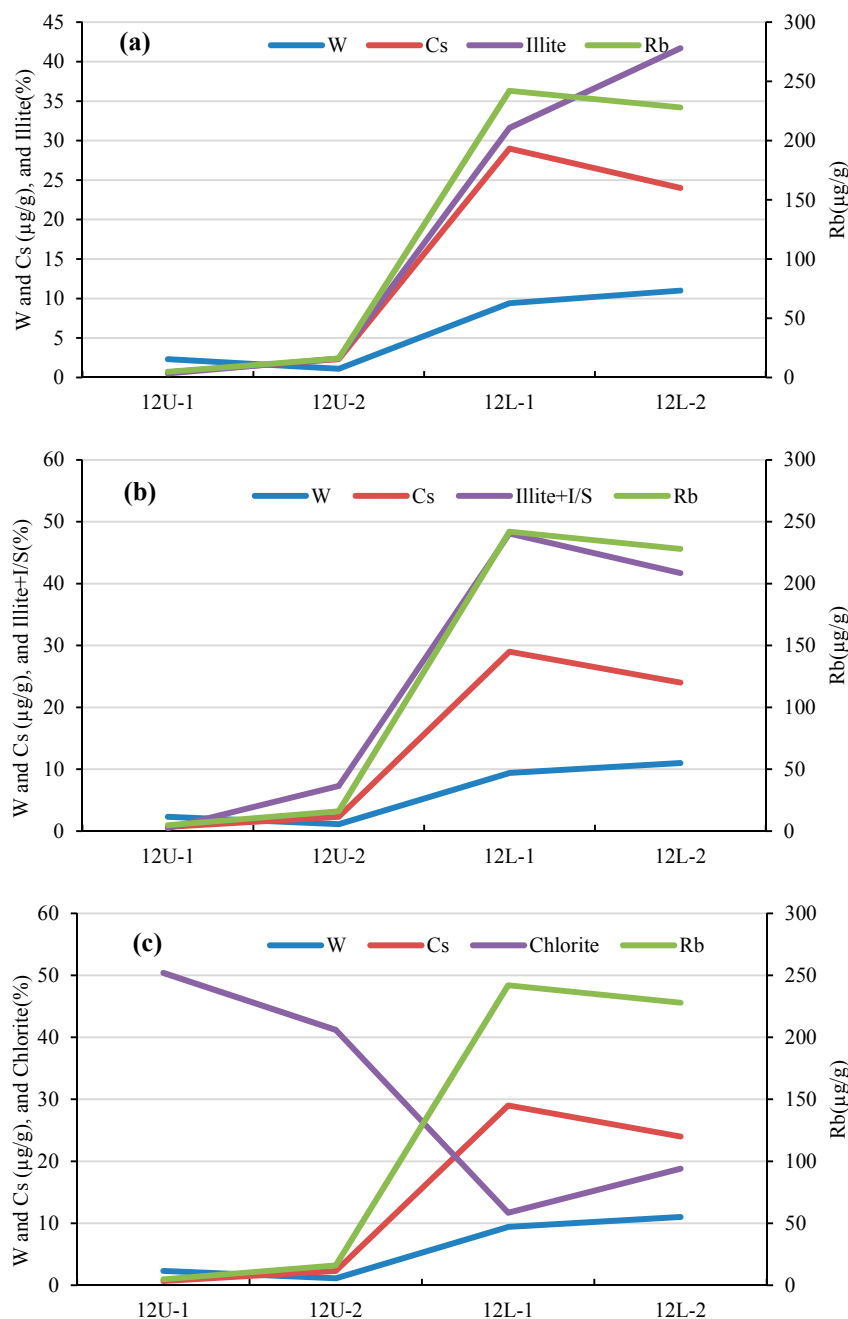


Figure 12. Relationship between W, Rb, and Cs and illite (a), illite + I/S (b), and chlorite (c) in the coals.

5.3.3. Tungsten

As discussed above, tungsten is significantly enriched in 12L Coal with a weighted average of $10.06 \mu\text{g/g}$ ($cc > 10$). Furthermore, elevated W is also found in the host rocks (Table 3), which might increase its potential economic significance for recovery. Up to now no one has set the exact and affirmative cut-off grades of W in coal. Many studies have indicated that organic matter in coals is the main carrier of W [4,10,57,60,63,64]. Moreover, some reports have shown that tungsten in coals can be associated with inorganic constituents, such as carbonate minerals [61] and quartz veins [1]. All these results indicate that W in coal is mainly associated with inorganic constituents and/or organic matter.

In this study, no tungsten minerals such as scheelite or ferberite occur in the coals to affect the W mass balance, indicating that tungsten in the coals is associated with inorganic constituents and/or organic matter. Compared with 12U Coal, 12L Coal exhibits a higher W concentration with a much greater ash yield (Tables 1 and 3), indicating that W is mainly associated with inorganic

matter [65]. Further study found that, just like Rb and Cs, higher concentrations of W in coals and host rocks are linked to higher K₂O contents and illite (Figures 11 and 12), confirming that illite may be the main carriers of W. The concentrations of W in illite of 12L Coal determined by SEM-EDX are 1.03%–3.15%, with an average of 1.85%, which also suggests this conclusion. In addition, a relatively high concentration of W in the 12L Coal has been detected in hydrothermal pyrite (1.32%–2.44%), with an average of 1.82%, which suggest that W in coal has a modest chalcophile tendency in bituminous coals and can occur in epigenetic sulfide mineralization [57].

5.3.4. Pb, Zn and Cd

As shown in Figure 3, Pb is significant enriched or slightly enriched in the studied coals. Some study results showed that lead in coals predominantly occur as micro-sized grains of galena and clausthalite [57,66]. In addition, many studies have reported that lead in coals predominantly occurs as sulfides or in association with sulfide minerals [61,67,68]. In this study, SEM-EDX analysis results indicated that hydrothermal pyrite may be the main carrier of Pb. The concentrations of Pb in hydrothermal pyrite determined by SEM-EDX are 3.05%–6.44%, with an average of 4.83%. In Table 3, it can be also seen that the concentration of Pb in 12U Coal is much higher than that in 12L Coal, which implies that there may be some micro-sized grains of galena and clausthalite in the coals, especially in 12U Coal.

In Figure 3, Zn and Cd are enriched or slightly enriched in the studied coals. It was reported that Zn and Cd in coals mainly occur in sphalerite [61,67]. In this study, no large sphalerite was found in the coals. In Table 3, it can be seen that the concentrations of Zn and Cd in 12L Coal are higher than that in 12U Coal, totally different from Pb, which seems to indicate that the mode of occurrence of Zn and Cd may be different from Pb in the studied coals. SEM-EDX analysis results can verify this point. It was showed that relatively high concentrations of Zn and Cd in the studied coals have been detected in hydrothermal illite, calcite, gypsum, and fluorite, indicating that these minerals may be the main carriers of Zn and Cd. In addition, traces of Zn were detected in hydrothermal pyrite, while Cd was below the SEM detection levels in pyrite.

5.4. Favorable Conditions for the Enrichment of W, Rb, and Cs in Coal

In this study, the magmatic hydrothermal fluids that penetrated the coals from the Meitian Mine extracted abundant rare metals (e.g., W, Rb, and Cs) from the granitic melts; this is predominantly ascribed to the following three aspects. (1) It is notable that granitic magmas contain abundant rare metals [49,50], which can later become concentrated in magmatic hydrothermal systems for eventual enrichment in coal. (2) Magmatic hydrothermal fluids contain abundant volatile matter (e.g., F, and CO₂), inferred by the hydrothermal fluorite and carbonate minerals (Figure 6d,g and Figure 7), which have very strong extraction and transporting capacities for rare metals (e.g., W) [69,70]. Therefore, magmatic hydrothermal fluids that are rich in volatile matter can extract abundant rare metals from granitic melts. (3) Temperature is closely related to the solubility of W in magmatic hydrothermal fluid [70,71]. The illitization and chloritization of the coal and the mineral assemblages of hydrothermal calcite, dolomite, tremolite, diopside, talc, and pyrite with combine crystal form in the coals (Figures 6 and 7) indicate that they formed at temperatures between 200 °C and 300 °C [56,72–74]. This is consistent with the fact that the decrepitation temperature of pyrite in coal metamorphism zone III shown in Figure 1c is approximately 250 °C [24]. Therefore, magmatic hydrothermal fluids with relatively high temperature can also extract abundant rare metals from granitic melts.

It is interesting that the concentrations of some elements in 12U and 12L Coals, especially W, Rb, and Cs, vary greatly (Figures 11 and 12). As discussed above, this variation is largely attributed to the much higher hydrothermal illite contents in 12L Coal than 12U Coal. However, the very distinct vertical zonality of altered illite in the coals (Figures 11 and 12) is worthy of further study. Some studies have shown that, in medium-low temperature hydrothermal altered environments, illite generally forms by illitization of plagioclase and mica, and is mainly affected by fluid influx, water/rock ratio,

temperature, and potassium contents in fluids [75–77]. The very distinct vertical zonality of illitization and chloritization in the coals (Figure 11) seems to indicate that limited fluid influx or a low water/rock ratio during water-rock interactions between magmatic hydrothermal fluids and coals might have restricted the formation of altered illite in upper 12U Coal, which can also be inferred from the decreasing percentage of K_2O through the vertical distribution of the coal (Figure 11). Considering the ascent of hydrothermal fluids, the decreasing fluid temperature may also have limited the formation of altered illite in 12U Coal. Therefore, our study results seem to suggest that hydrothermal alteration types in coal may be responsible for the enrichment of elements in coal intruded by magmatic rocks, which are mainly controlled by fluid influx, water/rock ratio, and fluid temperature. In addition, Eskenazy (1982) [47] reported that the pH value of magmatic hydrothermal fluids influences the enrichment of tungsten. However, the effects of fluid pH and Eh on rare metal enrichment in the coals require further study.

6. Conclusions

The 12U and 12L Coals from the Meitian Mine of southern China are late Permian low volatile anthracite coals, characterized by low (10.26%) and high ash coal (45.47%), respectively. The minerals in 12U Coal are predominantly chlorite, quartz, and calcite, while illite, quartz, chlorite, kaolinite, and mixed-layer illite/smectite (I/S) compose the minerals in 12L Coal. In addition, dolomite, fluorite, rutile, gypsum, tremolite, diopside, and talc are predominantly observed in 12L Coal using SEM-EDS techniques. Illite, chlorite, I/S, pyrite, and fluorite in the coals generally occur as vesicle and fracture fillings, indicating an epigenetic hydrothermal origin. Tremolite, diopside, and talc, which are uncommon in other coals, mainly occur as cleat-filling material in 12L Coal and probably formed from the reaction between dolomite and Si-rich magmatic hydrothermal fluids.

Pb (94.72 $\mu\text{g/g}$), Zn (101.76 $\mu\text{g/g}$), Sn (4.29 $\mu\text{g/g}$), and Cd (0.62 $\mu\text{g/g}$) are enriched or slightly enriched in 12U Coal, while W (10.06 $\mu\text{g/g}$), Rb (234.36 $\mu\text{g/g}$), and Cs (26.10 $\mu\text{g/g}$) are significantly enriched in 12L Coal. Furthermore, the host rocks are also rich in W, Rb, and Cs, which may increase their potential economic significance for recovery. REY plots for almost all coals, partings and host rocks are similar, showing an M-type REY distribution, Gd-maximum, positive Y anomalies, and negative Ce anomalies. Rubidium and cesium in the coals are clearly associated with K-rich clay minerals (illite + I/S), and some other hydrothermal silicate minerals (i.e., tremolite, diopside and talc). W in the coals mainly occurs in inorganic constituents (i.e., illite and pyrite), especially in illite. Hydrothermal pyrite, galena and clausthalite in the coals may be the main carrier of Pb, while Zn and Cd in the coals may be primarily associated with hydrothermal illite, calcite, gypsum, and fluorite.

The enrichment of W, Rb, and Cs in the coals is genetically associated with magmatic hydrothermal fluids. Magmatic hydrothermal fluids that are relatively high temperature and enriched in volatile matter can extract abundant W, Rb, and Cs from the granitic melts. Instead of other alterations (e.g., chloritization), the enrichment of these rare metals in the coal is mainly related to illitization of plagioclase and mica during water-rock interactions between magmatic hydrothermal fluids and coals. Our study results indicate that, for coal intruded by magmatic rocks, hydrothermal alteration types in coal may be responsible for the enrichment of elements, which are mainly controlled by fluid influx, water/rock ratio, and fluid temperature.

Author Contributions: Conceptualization, Z.X. and Y.C.; Data curation, Z.X. and Y.C.; Investigation, W.J., Y.H. and J.L.; Methodology, W.J., P.Z., Y.H. and J.L.; Writing—original draft, Z.X.

Funding: This research was funded by the National Natural Science Foundation of China (Grant No. 41603046), and the Natural Science Foundations of Hunan Province (Grant Nos. 2017JJ3070; 2018JJ2114).

Acknowledgments: Thanks are expressed to the editors and three anonymous reviewers, for their constructive comments and suggestions on the manuscript.

Conflicts of Interest: The authors declare no competing financial interest.

References

1. Dai, S.; Ren, D.; Chou, C.-L.; Finkelman, R.B.; Seredin, V.V.; Zhou, Y. Geochemistry of trace elements in Chinese coals: A review of abundances, genetic types, impacts on human health, and industrial utilization. *Int. J. Coal Geol.* **2012**, *94*, 3–21. [[CrossRef](#)]
2. Dai, S.; Wang, P.; Ward, C.R.; Tang, Y.; Song, X.; Jiang, J.; Hower, J.C.; Li, T.; Seredin, V.V.; Wagner, N.J.; et al. Elemental and mineralogical anomalies in the coal-hosted Ge ore deposit of Lincang, Yunnan, southwestern China: Key role of N₂-CO₂-mixed hydrothermal solutions. *Int. J. Coal Geol.* **2015**, *152*, 19–46. [[CrossRef](#)]
3. Zhao, C.; Liu, B.; Xiao, L.; Li, Y.; Liu, S.; Li, Z.; Zhao, B.; Ma, J.; Chu, G.; Gao, P.; et al. Significant enrichment of Ga, Rb, Cs, REEs and Y in the Jurassic No. 6 coal in the Iqe Coalfield, northern Qaidam Basin, China—A hidden gem. *Ore Geol. Rev.* **2017**, *83*, 1–13. [[CrossRef](#)]
4. Seredin, V.V.; Finkelman, R.B. Metalliferous coals: A review of the main genetic and geochemical types. *Int. J. Coal Geol.* **2008**, *76*, 253–289. [[CrossRef](#)]
5. Dai, S.; Xie, P.; Jia, S.; Ward, C.R.; Hower, J.C.; Yan, X.; French, D. Enrichment of U–Re–V–Cr–Se and rare earth elements in the Late Permian coals of the Moxinpo Coalfield, Chongqing, China: Genetic implications from geochemical and mineralogical data. *Ore Geol. Rev.* **2017**, *80*, 1–17. [[CrossRef](#)]
6. Seredin, V.V.; Dai, S. Coal deposits as potential alternative sources for lanthanides and yttrium. *Int. J. Coal Geol.* **2012**, *94*, 67–93. [[CrossRef](#)]
7. Hower, J.C.; Granite, E.J.; Mayfield, D.B.; Lewis, A.S.; Finkelman, R.B. Notes on contributions to the science of rare earth element enrichment in coal and coal combustion byproducts. *Minerals* **2016**, *6*, 32. [[CrossRef](#)]
8. Dai, S.; Finkelman, R.B. Coal as a promising source of critical elements: Progress and future prospects. *Int. J. Coal Geol.* **2018**, *186*, 155–164. [[CrossRef](#)]
9. Querol, X.; Alastuey, A.; Lopez-Soler, A.; Plana, F.; Fernandez-Turiel, J.L.; Zeng, R.; Xu, W.; Zhuang, X.; Spiro, B. Geological controls on the mineral matter and trace elements of coals from the Fuxin Basin, Liaoning province, northeast China. *Int. J. Coal Geol.* **1997**, *34*, 89–109. [[CrossRef](#)]
10. Finkelman, R.B.; Bostick, N.H.; Dulong, F.T.; Senftle, F.E.; Thorpe, A.N. Influence of an igneous intrusion on the inorganic geochemistry of a bituminous coal from Pitkin County, Colorado. *Int. J. Coal Geol.* **1998**, *36*, 223–241. [[CrossRef](#)]
11. Gurba, L.W.; Weber, C.R. Effects of igneous intrusions on coalbed methane potential, Gunnedah Basin, Australia. *Int. J. Coal Geol.* **2001**, *46*, 113–131. [[CrossRef](#)]
12. Jiang, J.; Cheng, Y.; Wang, L.; Li, W.; Wang, L. Petrographic and geochemical effects of sill intrusions on coal and their implications for gas outbursts in the Wolonghu Mine, Huaibei Coalfield, China. *Int. J. Coal Geol.* **2011**, *88*, 55–66. [[CrossRef](#)]
13. Yao, Y.; Liu, D. Effects of igneous intrusions on coal petrology, pore-fracture and coalbed methane characteristics in Hongyang, Handan and Huaibei Coalfields, north China. *Int. J. Coal Geol.* **2012**, *96–97*, 72–81. [[CrossRef](#)]
14. Salmachi, A.; Rajabi, M.; Reynolds, P.; Yarmohammadtooski, Z.; Wainman, C. The effect of magmatic intrusions on coalbed methane reservoir characteristics: A case study from the Hoskissons coalbed, Gunnedah Basin, Australia. *Int. J. Coal Geol.* **2016**, *165*, 278–289. [[CrossRef](#)]
15. Walker, R.; Mastalerz, M.; Brassell, S.; Elswick, E.; Hower, J.C. Chemistry of thermally altered high volatile bituminous coals from southern Indiana. *Int. J. Coal Geol.* **2007**, *71*, 2–14. [[CrossRef](#)]
16. Li, W.; Zhu, Y.; Chen, S.; Wang, H. The effects of igneous intrusions on coal-bed macerals, maturity, and adsorption. *Energy Sources Part A* **2017**, *39*, 58–66. [[CrossRef](#)]
17. Golab, A.N.; Carr, P.F. Changes in geochemistry and mineralogy of thermally altered coal, Upper Hunter Valley, Australia. *Int. J. Coal Geol.* **2004**, *57*, 197–210. [[CrossRef](#)]
18. Suárez-Ruiz, I.; Flores, D.; Marques, M.M.; Martinez-Tarazona, M.R.; Pis, J.; Rubiera, F. Geochemistry, mineralogy and technological properties of coals from Rio Maior (Portugal) and Peñarroya (Spain) Basins. *Int. J. Coal Geol.* **2006**, *67*, 171–190. [[CrossRef](#)]
19. Dai, S.; Ren, D. Effects of magmatic intrusion on mineralogy and geochemistry of coals from the Fengfeng–Handan Coalfield, Hebei, China. *Energy Fuels* **2007**, *21*, 1663–1673. [[CrossRef](#)]
20. Zheng, L.; Liu, G.; Qi, C.; Zhang, Y.; Wong, M. The use of sequential extraction to determine the distribution and modes of occurrence of mercury in Permian Huaibei coal, Anhui Province, China. *Int. J. Coal Geol.* **2008**, *73*, 139–155. [[CrossRef](#)]

21. Dai, S.; Zou, J.; Jiang, Y.; Ward, C.R.; Wang, X.; Li, T.; Xue, W.; Liu, S.; Tian, H.; Sun, X.; et al. Mineralogical and geochemical compositions of the Pennsylvanian coal in the Adaohai Mine, Daqingshan Coalfield, Inner Mongolia, China: Modes of occurrence and origin of diaspore, gorceixite, and ammonian illite. *Int. J. Coal Geol.* **2012**, *94*, 250–270. [[CrossRef](#)]
22. Chen, J.; Liu, G.; Li, H.; Wu, B. Mineralogical and geochemical responses of coal to igneous intrusion in the Pansan Coal Mine of the Huainan Coalfield, Anhui, China. *Int. J. Coal Geol.* **2014**, *124*, 11–35. [[CrossRef](#)]
23. Goodarzi, F.; Cameron, A.R. Organic petrology and elemental distribution in thermally altered coals from Telkwa; British Columbia. *Energy Sources* **1990**, *12*, 315–343. [[CrossRef](#)]
24. Wang, Y.; Mo, J.; Ren, D. Distribution of minor and trace elements in magmatic hydrothermal metamorphic coal of Meitian Coal Mine, Hunan Province. *Geochimica* **1999**, *28*, 289–296. (In Chinese with English abstract)
25. Ward, C.R. Analysis, origin and significance of mineral matter in coal: An updated review. *Int. J. Coal Geol.* **2016**, *165*, 1–27. [[CrossRef](#)]
26. Zhao, W.; Zhou, M.; Li, Y.; Zhao, Z.; Gao, J. Genetic types, mineralization styles, and geodynamic settings of Mesozoic tungsten deposits in South China. *J. Asian Earth Sci.* **2017**, *137*, 109–140. [[CrossRef](#)]
27. Li, Z.; Hu, R.; Yang, J.; Peng, J.; Li, X.; Bi, X. He, Pb and S isotopic constraints on the relationship between the A-type Qitianling granite and the Furong tin deposit, Hunan Province, China. *Lithos* **2007**, *97*, 161–173. [[CrossRef](#)]
28. Zhao, K.; Jiang, S.; Yang, S.; Dai, B.; Lu, J. Mineral chemistry, trace elements and Sr–Nd–Hf isotope geochemistry and petrogenesis of Cailing and Furong granites and mafic enclaves from the Qitianling batholith in the Shi-Hang zone, South China. *Gondwana Res.* **2012**, *22*, 310–324. [[CrossRef](#)]
29. Yang, Z. Correlation of the coal rock bed in the Meitian coalfield. *Coal Geol. Explor.* **1983**, *2*, 11–15. (In Chinese with English abstract)
30. ASTM Standards D3173-11. *Test Method for Moisture in the Analysis Sample of Coal and Coke*; ASTM International: West Conshohocken, PA, USA, 2011.
31. ASTM Standards D3174-11. *Annual Book of ASTM Standards. Test Method for Ash in the Analysis Sample of Coal and Coke*; ASTM International: West Conshohocken, PA, USA, 2011.
32. ASTM Standards D3175-11. *Test Method for Volatile Matter in the Analysis Sample of Coal and Coke*; ASTM International: West Conshohocken, PA, USA, 2011.
33. ASTM Standards D3177-02. *Test Method for Total Sulur in the Analysis Sample of Coal and Coke (Reapproved 2007)*; ASTM International: West Conshohocken, PA, USA, 2002.
34. ASTM Standards D2798-05. *Annual Book of ASTM Standards. Test Method for Microscopical Determination of the Vitrinite Reflectance of Coal, Gaseous Fuels, Coal and Coke*; ASTM International: West Conshohocken, PA, USA, 2005.
35. Han, T.; Zhu, X.; Li, K.; Jiang, L.; Zhao, C.; Wang, Z. Metal sources for the polymetallic Ni–Mo–PGE mineralization in the black shales of the Lower Cambrian Niutitang Formation, South China. *Ore Geol. Rev.* **2015**, *67*, 158–169. [[CrossRef](#)]
36. Chou, C.-L. Sulfur in coals: A review of geochemistry and origins. *Int. J. Coal Geol.* **2012**, *100*, 1–13. [[CrossRef](#)]
37. ASTM Standards D388-12. *Standards Classification of Coal by Rank*; ASTM International: West Conshohocken, PA, USA, 2012.
38. *Classification for Quality of Coal: Part 1. GB/T 15224.1-2018*; Standards Press of China: Beijing, China, 2018. (In Chinese)
39. Dai, S.; Seredin, V.V.; Ward, C.R.; Hower, J.C.; Xing, Y.; Zhang, W. Enrichment of U–Se–Mo–Re–V in coals preserved within marine carbonate successions: Geochemical and mineralogical data from the Late Permian Guiding Coalfield, Guizhou, China. *Miner. Depos.* **2015**, *50*, 159–186. [[CrossRef](#)]
40. Ketris, M.P.; Yudovich, Y. Estimations of Clarkes for Carbonaceous biolithes: World averages for trace element contents in black shales and coals. *Int. J. Coal Geol.* **2009**, *78*, 135–148. [[CrossRef](#)]
41. Bau, M.; Dulski, P. Distribution of yttrium and rare-earth elements in the Penge and Kuruman iron-formations, Transvaal Supergroup, South Africa. *Precambrian Res.* **1996**, *79*, 37–55. [[CrossRef](#)]
42. Dai, S.; Graham, I.T.; Ward, C.R. A review of anomalous rare earth elements and yttrium in coal. *Int. J. Coal Geol.* **2016**, *159*, 82–95. [[CrossRef](#)]
43. Taylor, S.R.; McLennan, S.M. *The Continental Crust: Its Composition and Evolution*; Blackwell: Oxford, UK, 1985; p. 312.

44. Cobb, J.; Steele, J.D.; Treworgy, C.G.; Ashby, J.F. The abundance of zinc and cadmium in sphalerite-bearing coals in Illinois. In *Illinois Mineral Note*; Illinois State Geological Survey: Champaign, IL, USA, 1980; Volume 74, p. 33.
45. Dawson, G.K.W.; Golding, S.D.; Esterle, J.S.; Massarotto, P. Occurrence of minerals within fractures and matrix of selected Bowen and Ruhr Basin coals. *Int. J. Coal Geol.* **2012**, *94*, 150–166. [[CrossRef](#)]
46. Dai, S.; Hower, J.C.; Ward, C.R.; Guo, W.; Song, H.; O’Keefe, J.M.K.; Xie, P.; Hood, M.M.; Yan, X. Elements and phosphorus minerals in the middle Jurassic inertinite-rich coals of the Muli Coalfield on the Tibetan Plateau. *Int. J. Coal Geol.* **2015**, *144–145*, 23–47. [[CrossRef](#)]
47. Eskenazy, G.M. The geochemistry of tungsten in Bulgarian coals. *Int. J. Coal Geol.* **1982**, *2*, 99–111. [[CrossRef](#)]
48. Dai, S.; Wang, X.; Seredin, V.V.; Hower, J.C.; Ward, C.R.; O’Keefe, J.M.K.; Huang, W.; Li, T.; Li, X.; Liu, H.; et al. Petrology, mineralogy, and geochemistry of the Ge-rich coal from the Wulantuga Ge ore deposit, Inner Mongolia, China: New data and genetic implications. *Int. J. Coal Geol.* **2012**, *90–91*, 72–99. [[CrossRef](#)]
49. Li, X.; Hu, R.; Bi, X.; Peng, J. Geochemistry and tin metallogenic potential for Qitianling granite mass in Southern Hunan. *J. Jinlin Univ.* **2010**, *40*, 80–92. (In Chinese with English abstract)
50. He, H.; Wang, D.; Su, X.; Zhang, Y.; Wang, G.; Li, J.; Zhao, B.; Li, J. Geochemical characteristics and ore potential of rare metal elements of the Qitianlin batholith in South Hunan, China. *Geotectonica Metallog.* **2014**, *38*, 366–374. (In Chinese with English abstract)
51. Kisch, H.J.; Taylor, G.H. Metamorphism and alteration near an intrusive coal contact. *Econ. Geol.* **1966**, *61*, 343–361. [[CrossRef](#)]
52. Dai, S.; Chou, C.-L.; Yue, M.; Luo, K.; Ren, D. Mineralogy and geochemistry of a Late Permian coal in the Dafang Coalfield, Guizhou, China: Influence from siliceous and iron-rich calcic hydrothermal fluids. *Int. J. Coal Geol.* **2005**, *61*, 241–258. [[CrossRef](#)]
53. Dai, S.; Zhang, W.; Seredin, V.V.; Ward, C.R.; Hower, J.C.; Song, W.; Wang, X.; Li, X.; Zhao, L.; Kang, H.; et al. Factors controlling geochemical and mineralogical compositions of coals preserved within marine carbonate successions: A case study from the Heshan Coalfield, southern China. *Int. J. Coal Geol.* **2013**, *109–110*, 77–100. [[CrossRef](#)]
54. Dai, S.; Xie, P.; French, D.; Ward, C.R.; Graham, I.T.; Yan, X.; Guo, W. The occurrence of buddingtonite in super-high-organic-sulphur coals from the Yishan Coalfield, Guangxi, southern China. *Int. J. Coal Geol.* **2018**, *195*, 347–361. [[CrossRef](#)]
55. Xie, L.; Wang, R.; Chen, J.; Zhu, J. Mineralogical evidence for magmatic and hydrothermal processes in the Qitianling oxidized tin-bearing granite (Hunan, South China): EMP and (MC)-LA-ICPMS investigations of three types of titanite. *Chem. Geol.* **2010**, *276*, 53–68. [[CrossRef](#)]
56. Pei, X.; Qian, Z.; Shi, G. A mineralogical study of the Chuncheon nephrite, South Korea. *Acta Petrol. Mineral.* **2011**, *30*, 89–94. (In Chinese with English abstract)
57. Finkelman, R.B.; Palmer, C.A.; Wang, P. Quantification of the modes of occurrence of 42 elements in coal. *Int. J. Coal Geol.* **2018**, *185*, 138–160. [[CrossRef](#)]
58. Yudovich, Y.; Ketris, M. *Valuable Trace Elements in Coal*; RAS: Ekaterinburg, Russia, 2006; p. 538.
59. Palmer, C.A.; Filby, R.H. Distribution of trace elements in coal from the Powhatan No. 6 mine, Ohio. *Fuel* **1984**, *63*, 318–328. [[CrossRef](#)]
60. Qin, S.; Lu, Q.; Li, Y.; Wang, J.; Zhao, Q.; Gao, K. Relationships between trace elements and organic matter in coals. *J. Geochem. Explor.* **2018**, *188*, 101–110. [[CrossRef](#)]
61. Swaine, D.J. *Trace Elements in Coal*; Butterworths: London, UK, 1990.
62. Seredin, V.V. Anomalous concentrations of trace elements in the Spetsugli Germanium Deposit (Pavlovka Brown Coal Deposit; southern Primorye): Communication 2. Rubidium and Cesium. *Lithol. Miner. Resour.* **2003**, *38*, 233–241. [[CrossRef](#)]
63. Seredin, V.V.; Danilcheva, Y.A.; Magazina, L.O.; Sharova, I.G. Ge-bearing coals of the Luzanovka Graben, Pavlovka brown coal deposit, southern Primorye. *Lithol. Miner. Resour.* **2006**, *41*, 280–301. [[CrossRef](#)]
64. Etschmann, B.; Liu, W.; Li, K.; Dai, S.; Reith, F.; Falconer, D.; Kerr, G.; Paterson, D.; Howard, D.; Kappen, P.; et al. Enrichment of germanium and associated arsenic and tungsten in coal and roll-front uranium deposits. *Chem. Geol.* **2017**, *463*, 29–49. [[CrossRef](#)]
65. Kortenski, J.; Sotirov, A. Trace and major element content and distribution in Neogene lignite from the Sofia Basin; Bulgaria. *Int. J. Coal Geol.* **2002**, *52*, 63–82. [[CrossRef](#)]

66. Dai, S.; Ren, D.; Chou, C.-L.; Li, S.; Jiang, Y. Mineralogy and geochemistry of the no. 6 coal (Pennsylvanian) in the Junger Coalfield, Ordos Basin, China. *Int. J. Coal Geol.* **2006**, *66*, 253–270. [[CrossRef](#)]
67. Finkelman, R.B. Modes of occurrence of potentially hazardous elements in coal: Levels of confidence. *Fuel Process. Technol.* **1994**, *39*, 21–34. [[CrossRef](#)]
68. Mastalerz, M.; Drobniak, A. Arsenic, cadmium, lead, and zinc in the Danville and Springfield coal members (Pennsylvanian) from Indiana. *Int. J. Coal Geol.* **2007**, *71*, 37–53. [[CrossRef](#)]
69. Linnen, R.L. The solubility of Nb-Ta-Zr-Hf-W in granitic melts with Li and Li+F: Constraints for mineralization in rare metal granites and pegmatites. *Econ. Geol.* **1998**, *93*, 1013–1025. [[CrossRef](#)]
70. O'Neill, H.S.C.; Berry, A.J.; Eggins, S.M. The solubility and oxidation state of tungsten in silicate melts: Implications for the comparative chemistry of W and Mo in planetary differentiation processes. *Chem. Geol.* **2008**, *255*, 346–359. [[CrossRef](#)]
71. Che, X.; Linnen, R.L.; Wang, R.; Aseri, A.; Thibault, Y. Tungsten solubility in evolved granitic melts: An evaluation of magmatic wolframite. *Geotectonics Metallog.* **2013**, *106*, 84–98. [[CrossRef](#)]
72. Lackschewitz, K.S.; Devey, C.W.; Stoffers, P.; Botz, R.; Eisenhauer, A.; Kummert, M.; Schmidt, M.; Singer, A. Mineralogical, geochemical and isotopic characteristics of hydrothermal alteration processes in the active; submarine, felsic-hosted PACMANUS field, Manus basin, Papua New Guinea. *Geotectonics Metallog.* **2004**, *68*, 4405–4427. [[CrossRef](#)]
73. Alekandre, P.; Kyser, K.; Polito, P.; Thomas, D. Alteration mineralogy and stable isotope geochemistry of paleoproterozoic basement hosted unconformity-type uranium deposits in the Athabasca Basin, Canada. *Econ. Geol.* **2005**, *100*, 1547–1563. [[CrossRef](#)]
74. Zhang, R.; Wang, Z.; Wang, S.; Liu, Y.; Qin, W. Metallogenic mechanism of Dayingezhuang gold deposit, northwestern Jiaodong Peninsula: Geochemistry constrains from the gold bearing pyrite typomorph and sulfur isotope. *Acta Petrol. Sin.* **2016**, *32*, 2451–2464. (In Chinese with English abstract)
75. Inoue, A.; Kitagawa, R. Morphological characteristics of illitic clay minerals from a hydrothermal system. *Am. Mineral.* **1994**, *79*, 700–711.
76. Jin, Z.; Zhu, J.; Ji, J.; Li, F.; Lu, X. Two origins of illite at the dexing porphyry Cu deposit; east China: Implications for ore-forming fluid constraint on illite crystallinity. *Clays Clay Miner.* **2002**, *50*, 381–387.
77. Brockamp, O.; Schlegel, A.; Wemmer, K. Complex hydrothermal alteration and illite K-Ar ages in Upper Viséan molasse sediments and magmatic rocks of the Variscan Badenweiler-Lenzkirch suture zone, Black Forest, Germany. *Int. J. Earth Sci.* **2015**, *104*, 683–702. [[CrossRef](#)]



© 2018 by the authors. Licensee MDPI, Basel, Switzerland. This article is an open access article distributed under the terms and conditions of the Creative Commons Attribution (CC BY) license (<http://creativecommons.org/licenses/by/4.0/>).